Composites Part B 203 (2020) 108463

Contents lists available at ScienceDirect

Composites Part B

journal homepage: www.elsevier.com/locate/compositesb

Towards the generation of controlled one-inch impact damage in thick CFRP composites for SHM and NDE validation

Robin James *, Victor Giurgiutiu

Department of Mechanical Engineering, University of South Carolina, 300 Main Street, Columbia, SC, 29208, USA

ARTICLE INFO

Keywords:
Carbon fiber reinforced polymer (CFRP) composite
Barely visible impact damage (BVID)
Quasi-isotropic
Impact testing
Structural health monitoring
Nondestructive evaluation
Ultrasonic testing
X-ray microCT
Surface profilometry

ABSTRACT

In this paper, an attempt has been made to conduct controlled low velocity impact experiments in quasi-isotropic carbon fiber reinforced polymer (CFRP) composites of increasing thicknesses to generate barely visible impact damage (BVID) that creates 1″ impact damage diameter. Such impacted CFRP coupons with controlled damage diameter would serve in the future for validation of structural health monitoring (SHM) and nondestructive evaluation (NDE) damage detection methodologies. Various 2-mm, 4-mm and 6-mm thick quasi-isotropic CFRP composite plates having similar stacking sequence were manufactured in a compression molding machine. These plates were cut into numerous 6″ × 4″ coupons to be impacted in accordance with ASTM D7136 standard on a Dynatup impact testing machine. The goal of the experiments was to identify the combination of impactor mass, energy and momentum at which approximately 1″ impact damage diameter could be produced for test coupons of increasing thicknesses. Interesting observations were made with respect to the size and shape of the impact damage as the thickness of the composite coupons was increased from 2-mm to 6-mm. Modified experiments were also conducted on 6-mm coupons to achieve close to 1″ impact damage diameter. The greatest challenge in conducting these experiments was in the thick 4-mm and 6-mm coupons which did not display a predictable trend. Future work should focus on overcoming this challenge towards achieving a predictable impact damage size methodology.

1. Introduction

1.1. STATE OF THE ART

In carbon fiber reinforced polymer (CFRP) composites, barely visible impact damage (BVID) can occur due to tool drops during manufacturing on the shop floor or low velocity impact of small and large debris during the service life of the structure. In low velocity impact events, the impactor may not penetrate the composite material but may still lead to BVID causing various types of damage such as delamination, matrix cracks and fiber fracture. BVID represents surface indentations which are too small to be seen during visual aircraft inspections and can cause the formation and growth of considerable internal damage. Under compressive loading scenarios such damage can propagate and can lead to extensive overall strength reduction of the composite structure.

The earliest work on impact testing of composites was conducted on unidirectional laminates in the 1970's by Butcher [1] and Toland [2] under different loading conditions to understand how an impact event affects the structural behavior of composites and how impact damage begins to propagate in composites. In the 1980's Cantwell et al. began to conduct low and high velocity impact tests on different stacking sequence of composites materials to see the influence of varies parameters like geometry and projectile mass on impact response of composites [3–7] Cantwell also began to look into methods that could be used to detect impact damage [8]. Subsequently researchers began to conform to ASTM standard of drop weight impact testing [9] for conducting their impact experiments. Ishai and Shragai [10] looked at the effect of impact loads on damage and residual compressive strength of CFRP laminated beams. Stellbrink [11] looked at the fatigue behavior of impact damaged CFRP laminates. After conducting impact experiments, it became important to come up with prediction models to quantify the residual strength of a composite after impact. This work was spearheaded by Caprino [12]. Shortly after prediction models were developed, finite element methods to model impact damage began to be explored by Clark [13] and other researchers [14–17]. In some recent work, Schoeppner et al. [18] investigated used low velocity impact load –time histories from the AFRL database to impact load level at which

* Corresponding author. , 300 Main Street, Columbia, SC, 29208, USA.
E-mail address: rj11@email.sc.edu (R. James).

https://doi.org/10.1016/j.compositesb.2020.108463
Received 31 July 2020; Received in revised form 23 September 2020; Accepted 4 October 2020
Available online 12 October 2020
1359-8368/

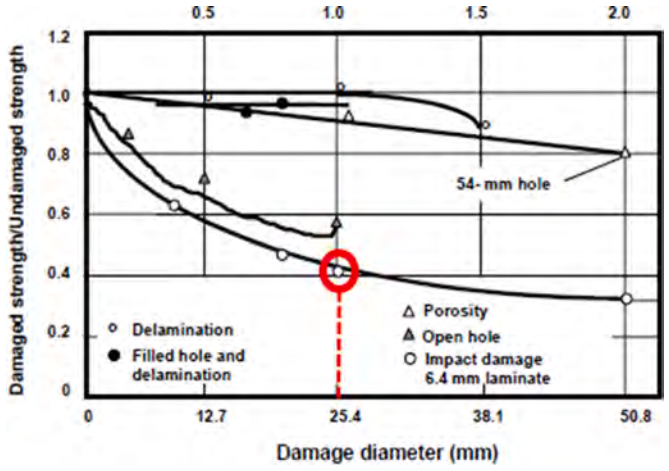

Fig. 1. Effect of impact damage diameter on compressive strength of composite [25].

impact damage will begin. Caputo et al. [19] developed numerical FEM models for impact scenarios in composites and proposed model described damage initiation and propagation of impact damage. Flores et al. [20] used 3D DIC to analyze the deformation in coupons subjected to low velocity impacts in the order of 10 J. Wallentine et al. [21] conducted serial sectioning microscopy and Ultrasonic scans to characterize BVID in unidirectional CFRP composites. Bogenfeld et al. [22] conducted a comprehensive review of impact analysis methods and discussed analytical and numerical models to predict impact damage and fiber failure. Panettieri et al. [23] conducted a benchmark low velocity impact study on thin 16-ply and 24-ply quasi-isotropic carbon/-epoxy laminates and proposed a numerical-experimental approach to evaluate the effect of impact energies. Gómez-del Río et al. [24] examined the effect of temperature on low velocity impact response of CFRP composites. Sutherland et al. [25] studied the impact response of marine laminates experimentally focusing on the energy absorption mechanisms of the laminates. Sevkat et al. [26] examined the effect of low velocity repeated impacts on plain-woven hybrid composites. Amaro et al. [27] investigated the influence of single and multiple impacts on GFRP composite laminates. Olsson [28] conducted analytical predictions of critical impact loads for large mass impact damage in 2-mm composite plates and validated them. This relationship was later used by Ghajari et al. [29] for the identification and reconstruction of impact force history for composite stiffened panels.

The concept of BVID was introduced in the 1980's with respect to understanding the damage tolerance of composite laminates [30,31]. In subsequent years, BVID became important in the inspection of composite aircraft where the damage needed to be characterized as BVID or visible impact damage (VID). BVID is defined as damage that is visible at a distance of less than 1.5 m and VID is defined as damage that is visible at a distance of 1.5 m or greater [32]. This clear distinction between BVID and VID during aircraft inspections can determine if a composite repair is needed or not. If a damage is characterized as VID it needs repairs to be conducted to the composite. However, there is a loophole to these definitions. A situation may arise where damage is characterized as BVID based on visual inspections but may have an impact damage diameter of 1″ or greater. An impact damage diameter of 1″ or greater may significantly deteriorate the compressive strength of the composite part (see Fig. 1) and may need immediate repairs and must not be discounted despite being characterized as BVID. From Fig. 1 we can also observe that in comparison to a 1″ damage diameter of any damage type (delamination, porosity, open hole), an impact damage having a diameter of 1″ or greater can significantly reduce the compressive strength of the composite structure. This is the significance and importance of detecting and monitoring impact damage having a diameter of 1″ or greater.

With the increasing occurrence of BVID in composites, detection methods needed to be developed to characterize the impact damage size and shape accurately. Ultrasonic testing was one of the first methods to be used for impact damage inspection and detection [8,33,34]. Guided wave propagation in composite laminates has been widely used as a structural health monitoring technique to observe the interaction of waves with impact damage over large propagation distances [35–38]. Eddy current methods have been explored by researchers to detect manufacturing flaws and operational damage such as impact damage in CFRP composites [39–41]. Researchers have also explored microwave nondestructive evaluation techniques to investigate low velocity and high velocity impact damage in composites due to environmental effects [42–45]. Infrared thermography is also being explored by scientists as a viable option of detecting impact damage in a rapid manner [46–48]. X-ray computed tomography is also being used by researchers to give a 3D assessment of impact damage in composite structures [49,50]. Advanced guided wave methods [51–54] are currently being explored by authors of this paper for rapid, reliable and large area assessment of composite structures subjected to controlled impact damage. The authors of this paper are also exploring the use of in-situ acoustic emission methods [55] for the ascertainment of extensive damage occurrence in impacted composites.

1.2. *Objectives of the current work*

The objective of this paper is to conduct controlled impact events in CFRP composite coupons of increasing thicknesses to produce a specific size of impact damage i.e. 1". Such impacted CFRP coupons with controlled damage diameter would serve in the future for validation of SHM and NDE damage detection methodologies. ASTM D7136 standard of impact testing has been used to conduct impact experiments on 6″ × 4″ quasi-isotropic coupons having a thickness ranging from 2-mm to 6-mm. The goal of the impact experiments was to identify a combination of mass, energy, and momentum of the impactor for which a controlled damage of 1″ can be produced. Ultrasonic testing and X-ray micro-CT was used to visualize the size and extent of impact damage that was produced in each experiment. Surface profilometry was used to examine the impacted surface of the composite coupon as well as the rear surface of the composite coupon. The results demonstrate that controlled damage is much easier to be obtained in thin laminates compared to thicker laminates [56]. Currently, to validate SHM and NDE detection methods, embedded simulated delaminations are employed in between layers of laminated composite materials by using thin sheets of Teflon or Mylar [57]. Our approach gives us an opportunity to create a specific size of real impact damage as compared to simulated damages for effective and accurate SHM and NDE validation.

2. Manufacturing of quasi-isotropic CFRP composite plates

To make the coupons for impact testing, composite plates were manufactured using the CYCOM ® 5320–1 epoxy resin system with the Hexcel IM7 12 K fiber in a compression molding (hot press) machine with the manufacturer's cure cycle. To manufacture quasi-isotropic composite plates with different thicknesses an appropriate stacking sequence with the appropriate number of layers had to be chosen. The quasi-isotropic stacking sequence was chosen based on the work done by previous researchers [19,20]. A $[-45/90/+45/0]_{2S}$ stacking sequence was chosen for manufacturing the 2-mm composite plate with 16 layers. To manufacture a 4-mm composite plate, a $[-45/90/+45/0]_{4S}$ stacking sequence with 32 layers was chosen and to manufacture a 6-mm composite plate a $[-45/90/+45/0]_{6S}$ stacking sequence with 48 layers was chosen. After the manufacturing process in the compression molding machine, the thickness of the manufactured plates was a little higher than anticipated, i.e. the 2-mm plate had an average thickness of 2.14 mm, the 4-mm plate had an average thickness of 4.15 mm and the 6-mm

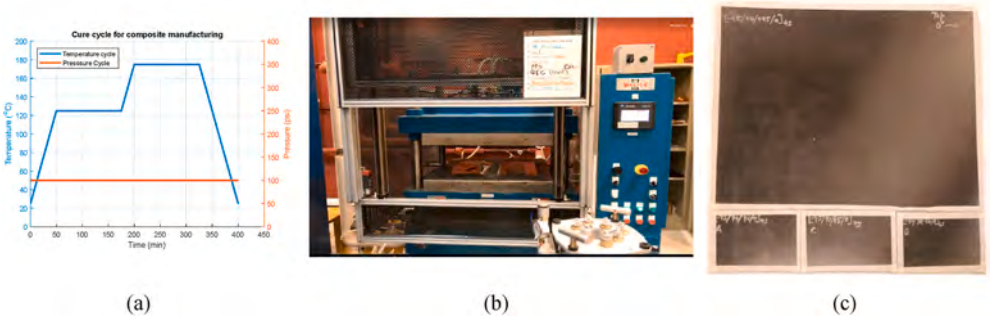

Fig. 2. Manufacturing of quasi-isotropic composite plates: (a) Cure cycle; (b) compression molding machine; (c) Final composite plate with 6″ × 4″ cut-outs.

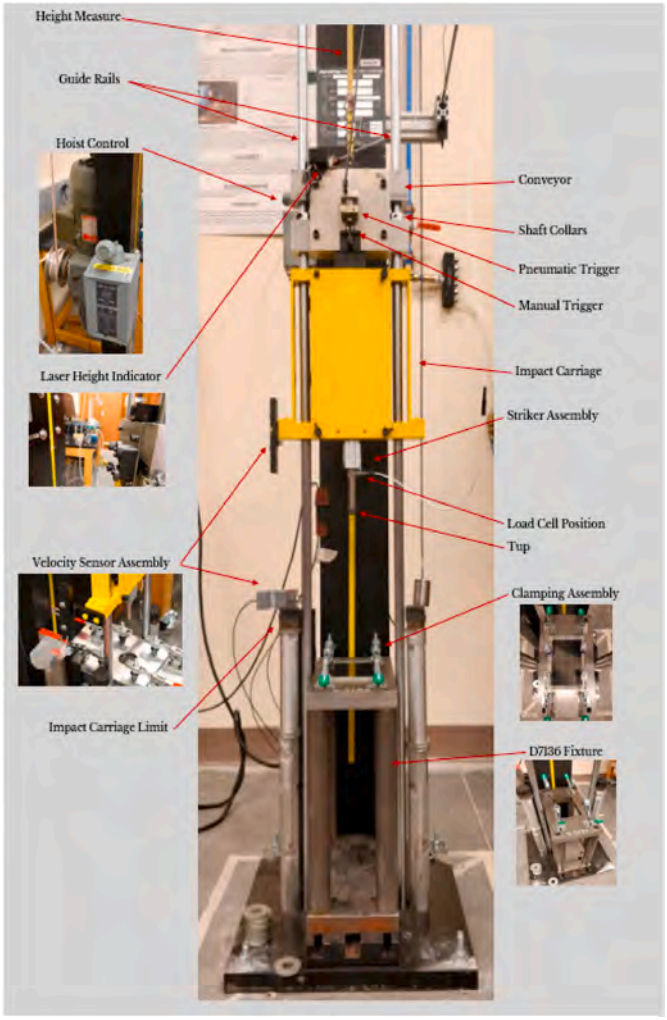

Fig. 3. Dynatup 8200 drop weight impact testing machine.

plate had an average thickness of 6.28 mm. The plates that were manufactured were cut into 6″ × 4″ coupons to conduct impact tests conforming to the ASTM D7136 standard of impact testing. The cure cycle, compression molding machine and one of the manufactured composite plates is displayed in Fig. 2. From the large composite plates, the 6″ × 4″ standard size coupon for the ASTM D7136 testing was cutout as displayed in Fig. 2 (c).

3. Experimental procedures

3.1. ASTM D7136 drop weight impact testing

A drop tower with low friction guide rails is used to induce collision between a mass of known weight (impactor) and a fixed composite coupon of dimensions 6″ × 4". The controlled impact event is recorded by a piezoelectric load cell which can accurately record data of the applied impact force, energy absorbed by the coupon and the displacement of the coupon during the event. Using variable impact heights, data is collected that shows how the coupon behaves under impacts of varied magnitude, and these impact tests can be conducted in sequence to see how damage forms in the coupon over repeated impacts. This data can then be used to predict future behavior of the material such as crack propagation and other damage formation. These tests are particularly useful when studying composite materials. Since composites are designed to distribute damage throughout the volume of a material, damage formation and the propagation of cracks can be difficult to predict accurately through theory and simulation alone. Also, difficulties in predicting important properties such as stiffness of the material and the amount of energy it is capable of absorbing before experiencing failure make drop weight impact testing a valuable process in material science.

Before the test is conducted, it is important to make sure that the impact carriage and conveyor is secured safely above the clamping platform. The sample is placed on top of the support fixture centering it on top of the 5″ × 3″ cut-out and the assembly is clamped into place. A protective cover is placed over the coupon to prevent accidental damage. After this the conveyor is slowly raised or lowered using the hoist control to the desired distance above the sample and is fastened into place using the shaft collars. This distance is measured using the laser height indicator and determines the drop height. All the equipment is checked to ensure that the data acquisition system is recording the data properly and then it is engaged; also checked is that the sample cover is removed. The trigger mechanism is then activated, initiating the drop impact event. The impactor can be caught safely after rebounding from the coupon to avoid secondary impact. It is also possible to avoid secondary impact if the drop weight impact testing machine has an anti-rebound device or stop block. The data is saved and the impact carriage is lifted away from the sample and is locked back into place on the conveyor. The sample cover is placed over the coupon to ensure no further damage to it as the conveyor's shaft collars are unlocked and the hoist mechanism is used to lift the carriage away from the clamping

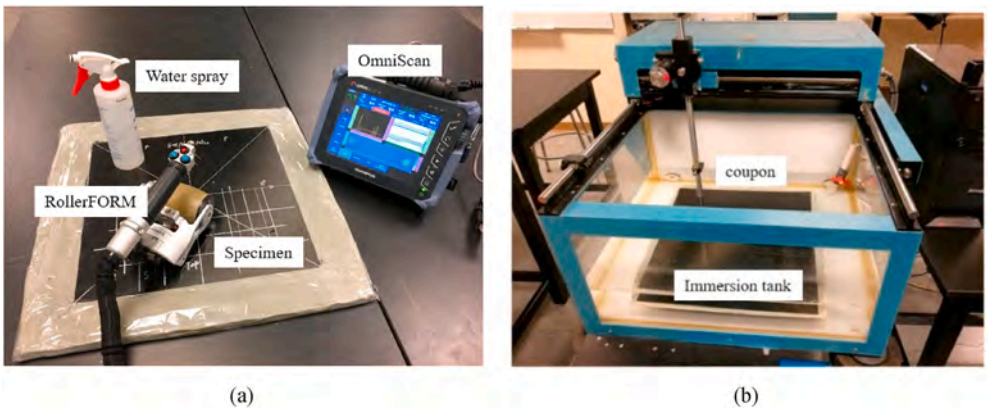

Fig. 4. UT scans were performed using (a) RollerFORM inspection (b) Immersion tank inspection.

assembly. The entire experimental setup is displayed in Fig. 3.

3.2. ULTRASONIC NDE OF IMPACTED COUPONS

Ultrasonic testing (UT) scans were conducted using the RollerFORM inspection and also in the ultrasonic immersion tank on the CFRP composite coupons before and after impact to obtain the B-scan and C-scan images and compare a pristine coupon with a coupon that underwent impact damage and to see the size and shape of the impact damage. In the case of the RollerFORM inspection, a thin layer of water is sprayed on the composite coupons to be inspected and a phased array wheel probe is moved along the composite coupon and the B-scan and C-scan images of the scanning area are displayed on the OmniScan system. In the case of the immersion tank inspection, a 10 MHz, 1″ focused, 0.375″ diameter ultrasonic transducer was used in the pulse-echo mode for conducting the UT scans. Post-processing of the data obtained from the ODIS software interface is able to give us a clear C-scan image, B-scan image, and A-scans in the pristine and impacted coupons. The experimental setups for these inspection techniques are displayed in Fig. 4.

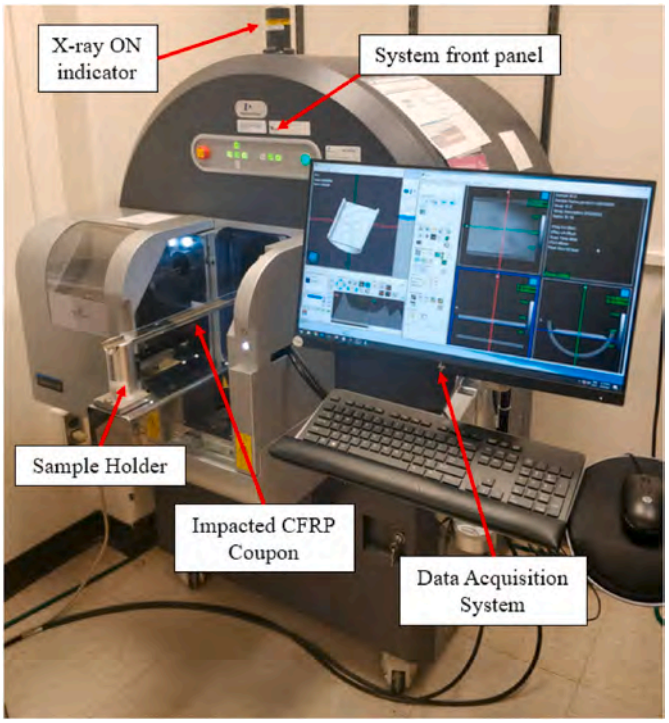

Fig. 5. PerkinElmer Quantum GX microCT Imaging System.

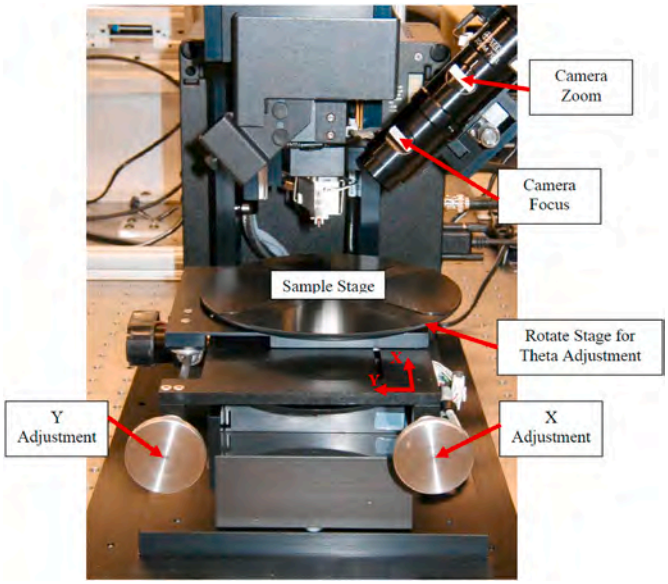

Fig. 6. Veeco Dektak 3ST surface profiler.

3.3. X-RAY MICRO COMPUTED TOMOGRPAHY OF IMPACTED COUPONS

To visualize some of the internal features of the impact damage that were not clearly visible using the ultrasonic NDE technique, X-ray micro-CT (computed tomography) technique was used. The Quantum GX microCT imaging system from PerkinElmer as displayed in Fig. 5 was used for imaging the impacted 2-mm, 4-mm and 6-mm CFRP coupons.

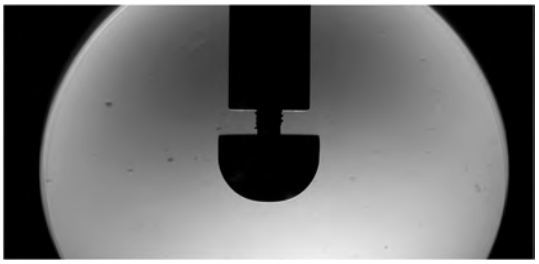

Fig. 7. Shadowgraph of the impactor tup.

Table 1
Impact tests conducted on 2-mm quasi-isotropic coupons.

Coupon	Avg. thickness (mm)	Mass (kg)	Height (cm)	Energy (J)	Impact velocity (m/s)	Momentum (Ns)	Damage size (in)	Ei (J)	% of Ei absorbed
B	2.15	3.059	19.512	5.855	1.791	5.478	0.6	4.906	64
C	2.13	3.059	19.512	5.855	1.772	5.420	0.63	4.802	52
D	2.11	3.059	32.194	9.661	2.204	6.740	0.77	7.427	67
E	2.19	3.059	32.194	9.661	2.209	6.757	0.8	7.463	69
F	2.14	3.059	46.828	14.052	2.626	8.034	0.95	10.550	61
G	2.02	3.059	46.828	14.052	2.679	8.193	0.93	10.972	60
H	2.19	3.059	53.462	16.042	2.858	8.743	1.015	12.495	54
I	2.17	3.059	53.462	16.042	2.899	8.866	1.04	12.850	65

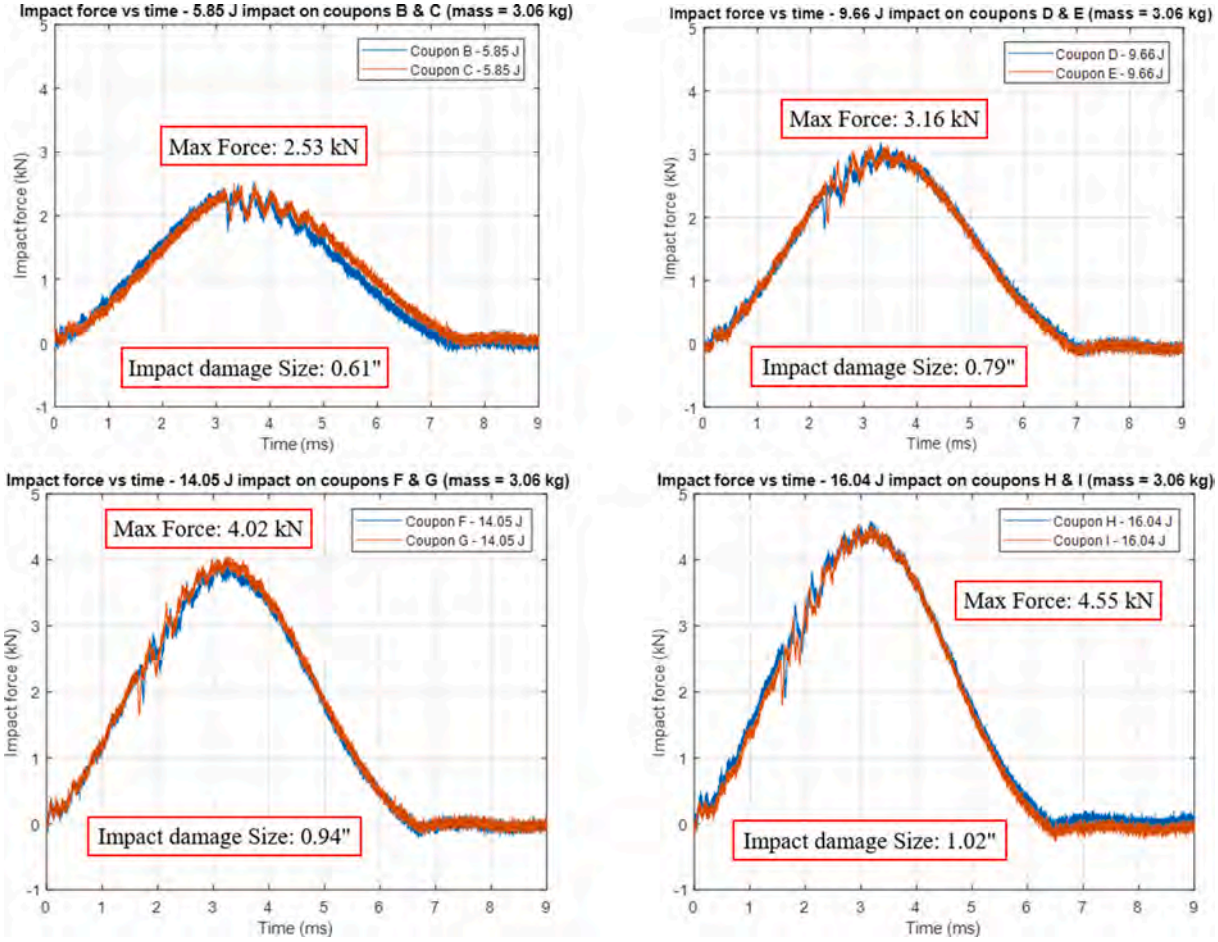

Fig. 8. Force-time history of $[-45/90/+45/0]_{2S}$ coupons.

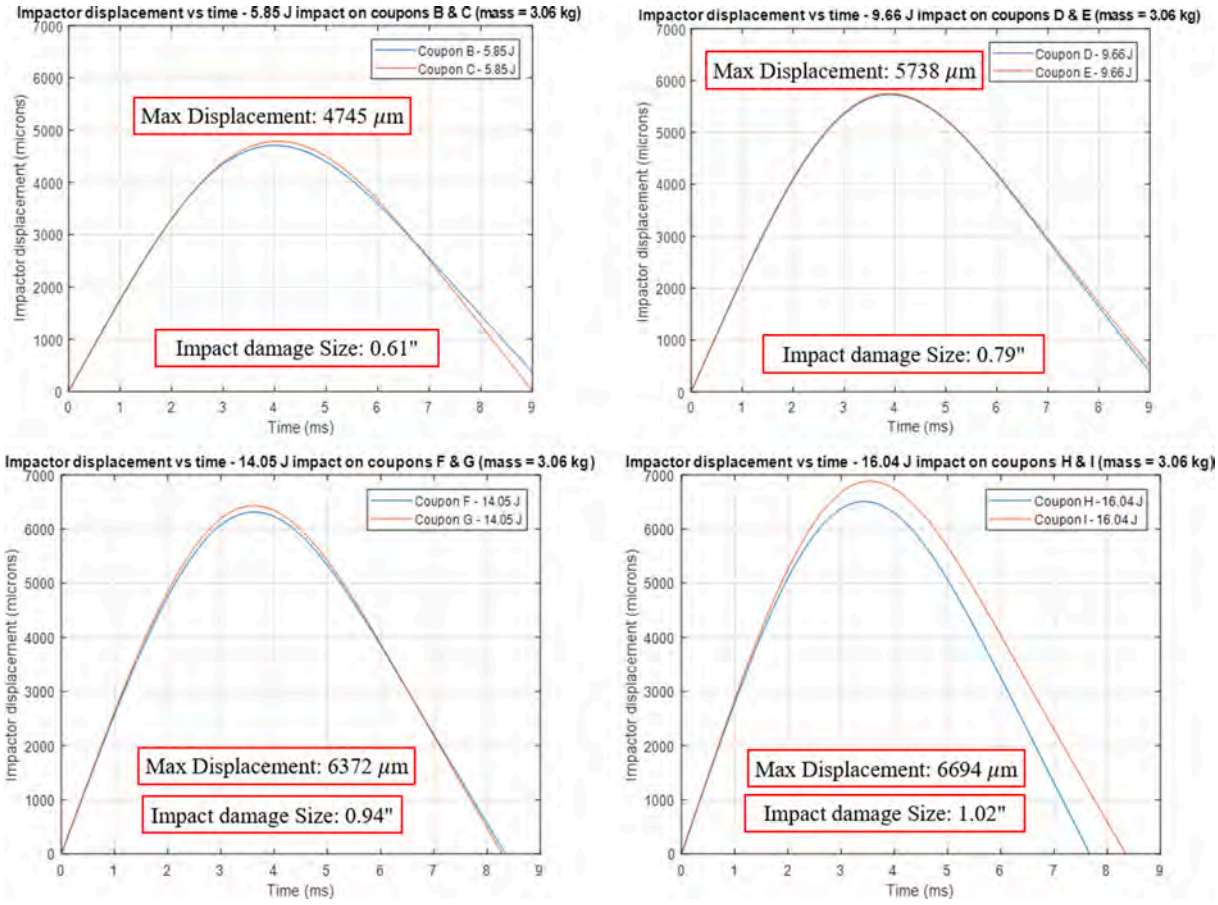

Fig. 9. Displacement-time history of $[-45/90/+45/0]_{2S}$ coupons.

Different sizes of sample beds can be used to accommodate different size of specimens. The impacted 6″ × 4″ coupons can also be accommodated. However, to image the impacted area more clearly with a smaller field of view and a smaller voxel size, representative impacted coupons with desirable impact damage were cut into smaller sizes for better resolution of images.

3.4. *SURFACE PROFILOMETRY OF IMPACTED COUPONS*

When a CFRP structure undergoes a BVID, the changes in surface profile are not apparent. In addition to visualizing the internal damage inside the composite structure, it is important to look at the changes in the surface profile of the structure as well. In order to do this, a Veeco Dektak 3ST surface profiler as displayed in Fig. 6 was used to conduct profilometry scans on impacted coupons. These profilometry scans were useful in determining the dent depth of the top surface i.e. impacted surface of the coupons as well as determining the pushout depth of the back surface of the coupons. The surface profile also elucidates the shape of the impactor tup which is hemispherical as can be seen from the shadowgraph image as displayed in Fig. 7.

4. Analysis of impact testing data

Behavior of a sample during the impact event can be observed in the data that is recorded from the load cell. The impact force-time history is converted from the load cell output voltage. Following ASTM D7136 [9], the impact velocity is calculated by:

$$v_i = \frac{w_{12}}{(t_2 - t_1)} + g\left(t_i - \left(\frac{t_1 + t_2}{2}\right)\right) \quad (1)$$

Where w_{12} = distance between flag prongs, t_1, t_2 = time first and second flag prong passes detector, g = acceleration due to gravity, and t_i = time

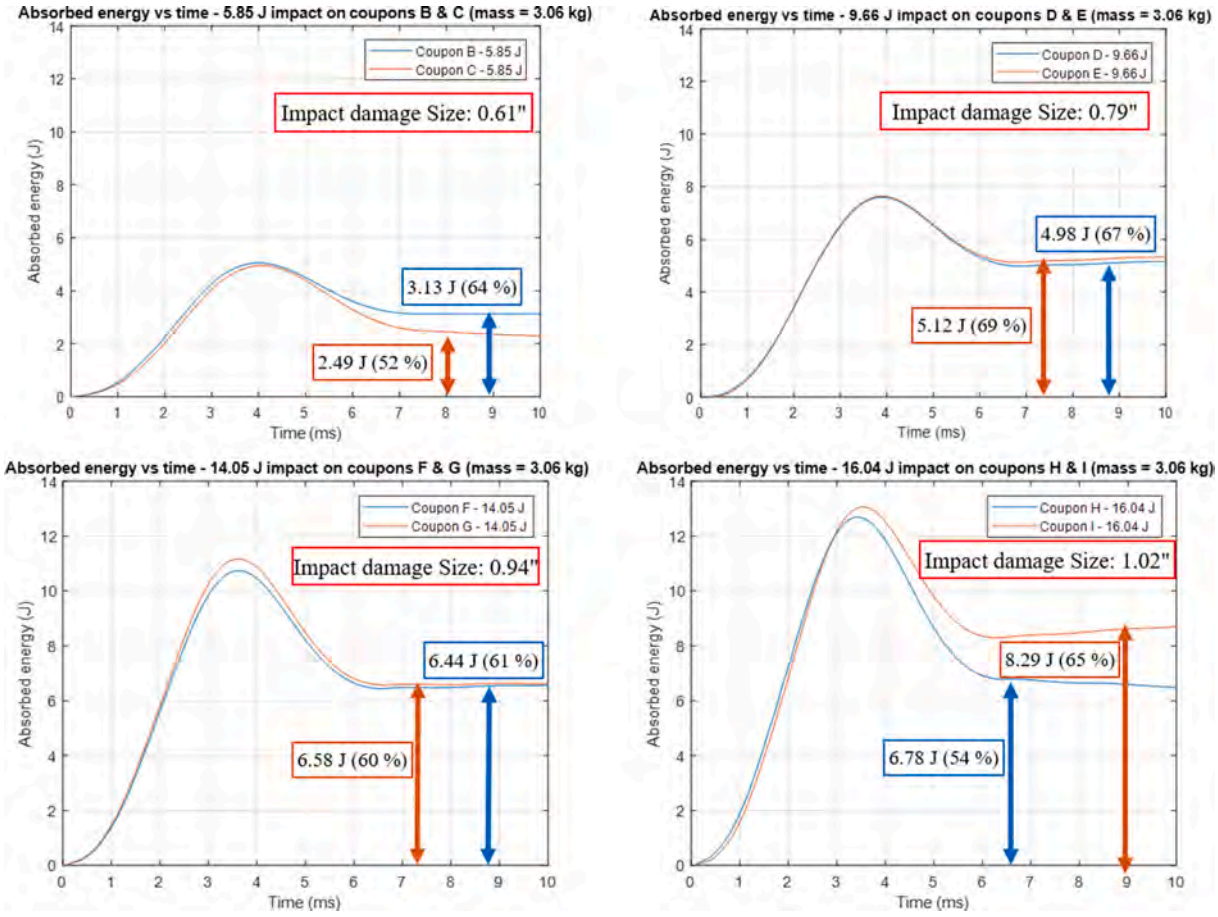

Fig. 10. Energy-time history of $[-45/90/+45/0]_{2S}$ coupons.

of initial contact.

The velocity and displacement history of the impactor is calculated by:

$$v(t) = v_i + gt - \int_0^t \frac{F(t)}{m} dt \tag{2}$$

$$\delta(t) = v_i t + \frac{gt^2}{2} - \int_0^t \left(\int_0^t \frac{F(t)}{m} dt \right) dt \tag{3}$$

Where v_i = impact velocity, t = time, F = impact force, and m = mass of impactor. Furthermore, the energy absorbed by the coupon can be calculated using:

$$E_a(t) = \frac{m\left(v_i^2 - v(t)^2\right)}{2} + mg\delta(t) \tag{4}$$

This data provides insight into how the sample performs under the stresses applied by the impact weight and can preview how the sample absorbs energy and how damage propagates. Questions about how brittle the sample is and whether it was destroyed during the impact event can be indicated by the force-time curve.

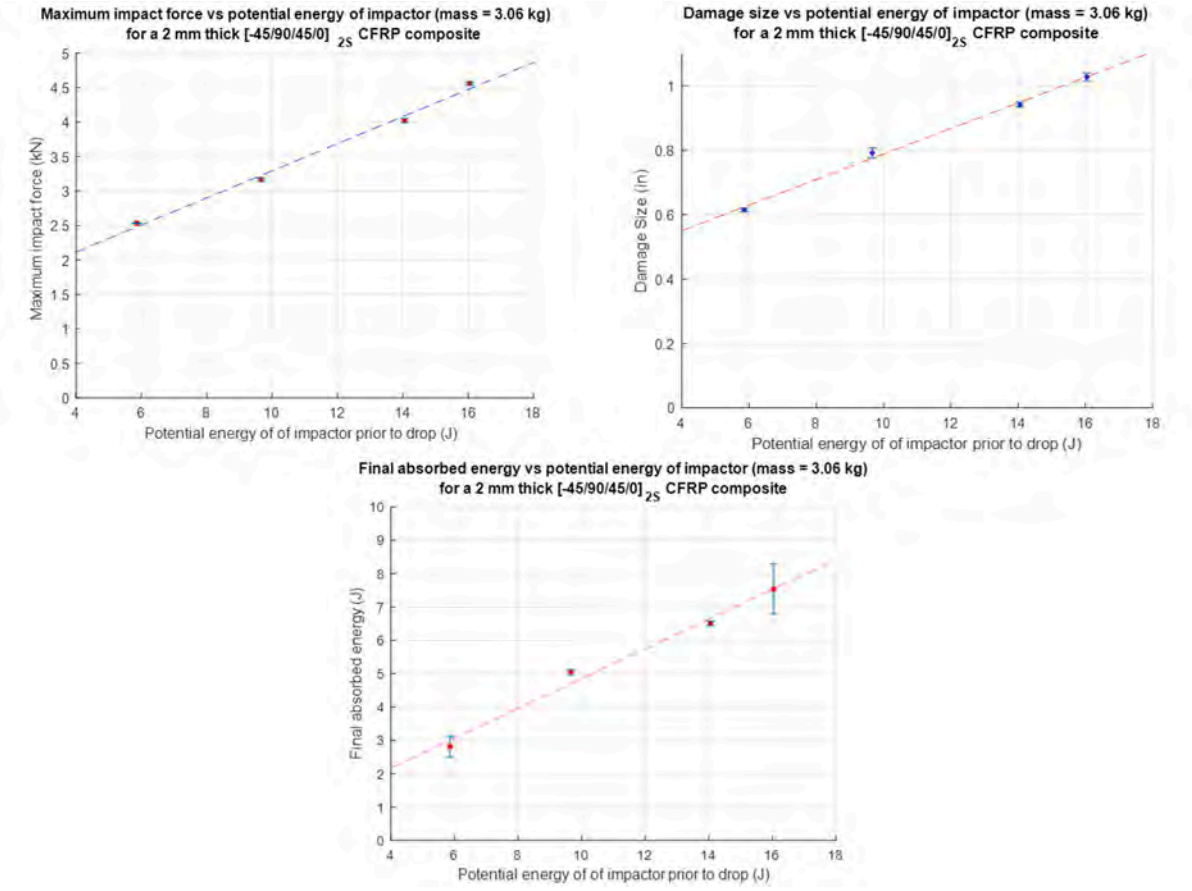

Fig. 11. Maximum impact force, impact damage size and absorbed enrgy of $[-45/90/+45/0]_{2S}$ coupons.

5. Experimental results

5.1. Impact tests conducted on 2-mm quasi-isotropic coupons

Impact tests were conducted on various 6″ × 4″ coupons having the stacking sequence of $[-45/90/+45/0]_{2S}$ which had thickness in the range of approximately 2-mm. The details of the impact tests are given in Table 1. This table indicates that 2 coupons were used for the same potential energy with an impactor mass of 3.06 kg. Coupons B and C were impacted with 5.85 J, coupons D and E were impacted with 9.66 J, coupons F and G were impacted with 14.05 J and coupons H and I were impacted with 16.04 J. All the energies were incremental and were estimated to try and obtain 1″ impact damage diameter in the 2-mm thick coupons in an iterative process. In coupons H and I with impactor energy of 16.04 J we were able to obtain 1″ impact damage diameter.

The force-time history of the impacts is given in Fig. 8. The load curve shows peaks at certain maximum load and is parabolic in shape. When the load curve is symmetric, its shape indicates that the impact energy is primarily deflected and little or no damage has occurred in the coupon. When there are irregularities in the parabolic shape of the load curve this indicates that the coupon has undergone extensive damage.

The velocity-time history of the impact events in the 2-mm coupons begins from being positive initially as the impactor is dropped towards the coupon then it becomes zero upon contacting the coupon and becomes negative as the impactor rebounds from the coupon and moves upwards. The negative velocity indicates the upward rebounding of the impactor after impacting the coupon. The displacement-time history of the coupons begins from zero and becomes maximum upon contacting with the impactor and then goes back to zero as the impactor is rebounded upwards as can be clearly observed in Fig. 9. We can clearly observe that the maximum displacement is obtained in coupons H and I

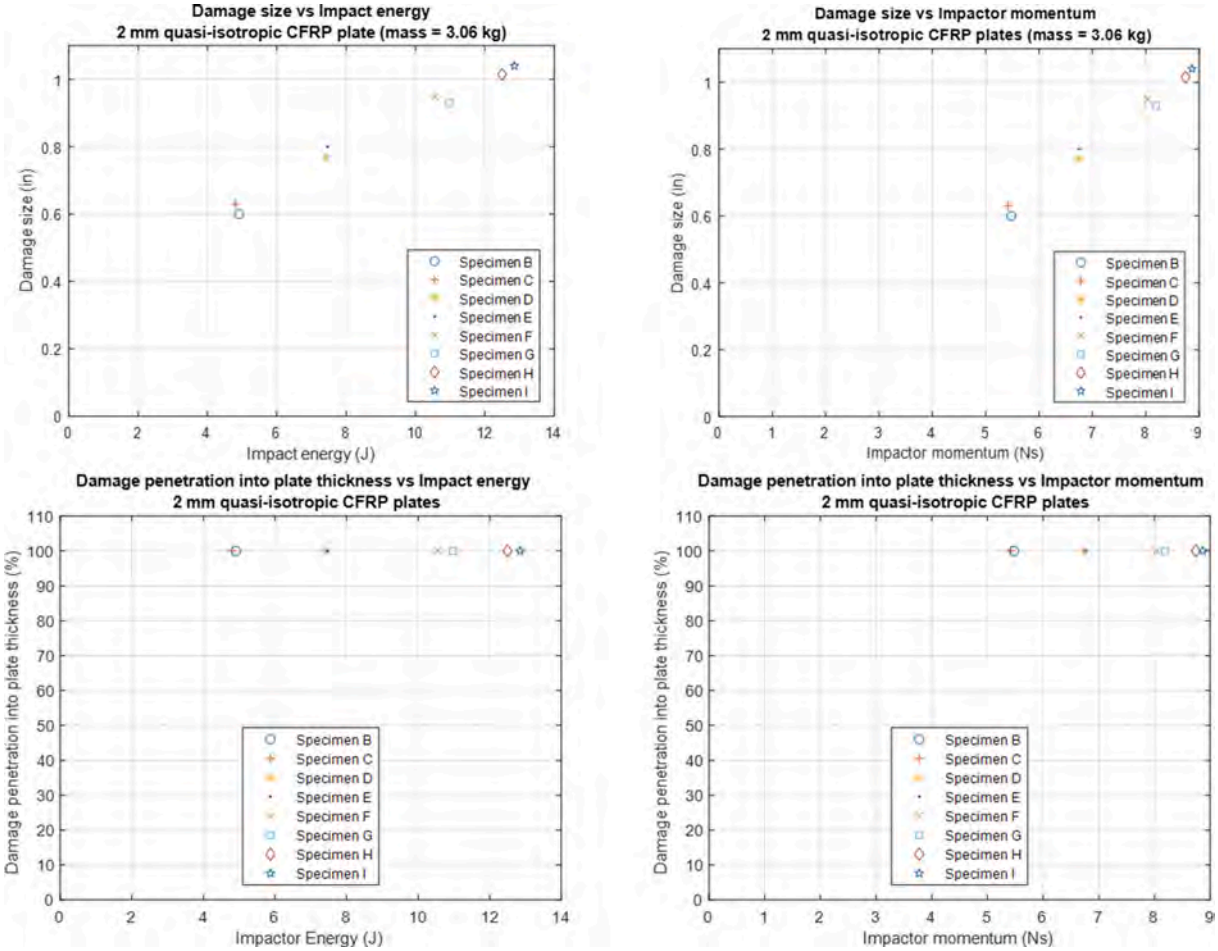

Fig. 12. Effect of impact energy and momentum on impact damage size in $[-45/90/+45/0]_{2S}$ coupons.

for an impact energy of 16.04 J. which causes an internal delaination size of 1".

The energy-time plots given in Fig. 10 are taken from the force-time curves through integration of the data. The energy-time plots better describe the peak energy experienced and energy absorbed by the coupons. Here, the energy absorbed is the difference between the value at the end of the plot and the initial value. The difference between the peak energies observed and the energy absorbed can be used to determine the efficiency of energy absorption by the material. Furthermore, the energy-time history clearly is able to demonstrate the percentage of impact energy that is absorbed by the coupon to create the irreversible process of damage. For coupons H and I where 1″ impact damage diameter is formed, over 65% of the impact energy is absorbed by the coupons.

After performing two impact tests per energy/drop height, the data obtained was further extrapolated to obtain a linear relationship between maximum impact force and potential energy of impactor. A linear relationship was also obtained between impact damage sizes and potential energy of impactor. Similarly, a linear relationship was also obtained between the absorbed energy and potential energy of impactor. These relationships are displayed in Fig. 11. From these impact experiments, we can also infer the effect of impact energy and impact momentum on impact damage size and penetration of damage across the thickness of these coupons as indicated in Fig. 12. Hence a mass, height and energy combination of the impactor was obtained to initiate a 1″ size impact damage in a $[-45/90/+45/0]_{2S}$ 2-mm thick quasi-isotropic coupon.

Ultrasonic immersion tank scans were conducted to obtain the B-

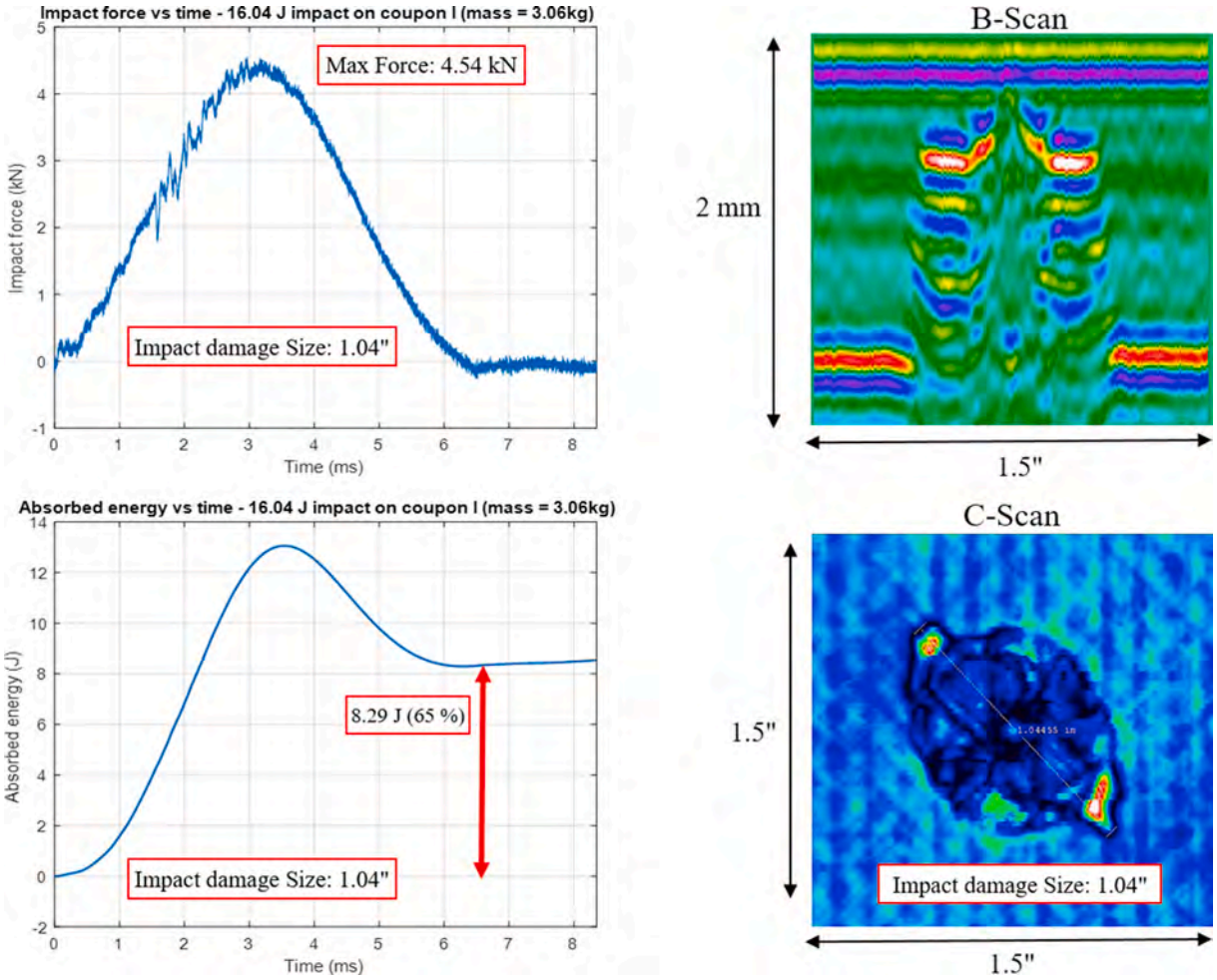

Fig. 13. Quad plot of 2-mm coupon with force-history, energy-history, B-scan and C-scan.

scan and C-scan images of the impact damage to observe its shape and size. From the B-scan, it can be seen that although, the center of the damage area undergoes permanent deformation similar to a dent, it does not have a delamination as a clear reflection from the center of the damage can be seen in the B-scan. From the C-scan image, we can clearly see the fiber cracking and pushout in the -45° fiber direction and this can be seen by looking at the rear surface of the coupon. A quad plot of coupon I, displaying the force-time history, the energy time history, The B-scan and C-scan is observed in Fig. 13.

X-ray micro-CT imaging was conducted to obtain slices of the impact damage as it propagates from the top surface of the coupon to the bottom surface in a "rotating fan" phenomenon. The C-scan image (X–Y plane) at one of the bottom layers is displayed in Fig. 14 (a) along with the green dashed line and the blue dashed line which are the locations along which the B-scan images have been produced. The B-scan images of both the Z-X plane (Fig. 14 (b)) and the Y-Z plane (Fig. 14 (c)) can also be observed. From the B-scan images in can be observed that the center of the impact damage has a pyramidal shape and is composed of many matrix cracks and small delaminations in the form a staircase like transition.

Profilometry scans of coupon I which produced a 1″ damage were conducted using a Veeco Dektak 3ST surface profiler to observe the profile of the top and bottom surface after impact. The profilometry images are displayed in Fig. 15. Using the top surface scan we were able to estimate that the dent depth is approximately 54 μm and using the bottom surface scan we were able to estimate the pushout height as 80 μm. Some of the irregularities in Fig. 15 (b) can be attributed to the rough bottom surface of the composite. This roughness appears due to

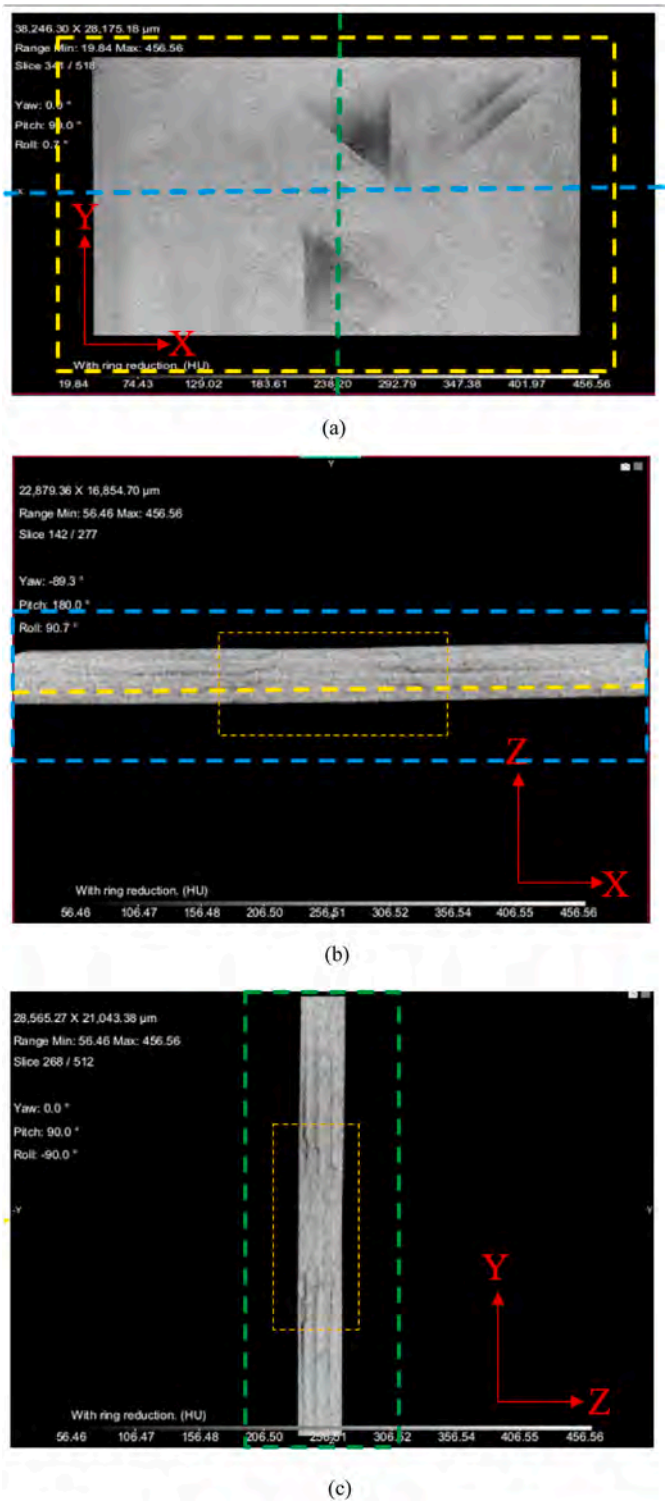

Fig. 14. X-ray micro-CT of 2 mm coupon with 1″ impact damage.

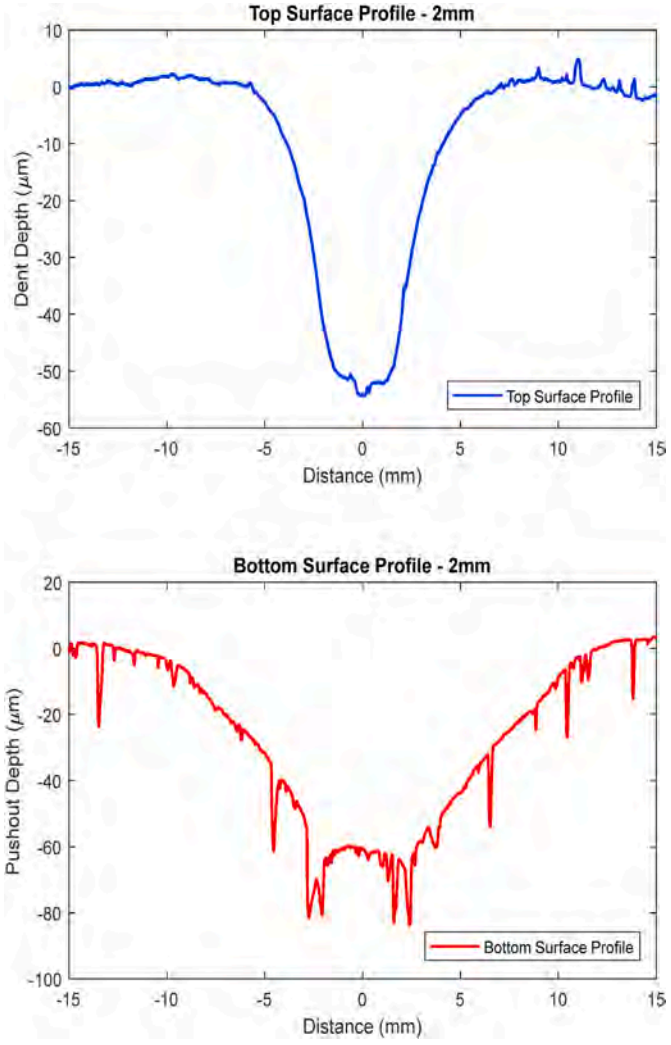

Fig. 15. Profilometry scans of 2-mm coupon: (a) Top surface; (b) Bottom surface.

the fact that the caul plates used to manufacture this coupon were not smooth and the impressions on the surfaces of the caul plates were imprinted on the coupon thereby making it rough with irregularities. This roughness was fixed in subsequent manufacturing of the composite plates. It is also interesting to observe that the dent profile seems hemispherical with a small dimple. The dimple is attributed to the tup which was used for the impact and was not ground well.

5.2. Impact tests conducted on 4-mm quasi-isotropic coupons

Similar to the previous section, impact tests were conducted on various 6″ x 4” coupons having the stacking sequence of $[-45/90/+45/0]_{4S}$ which had thickness in the range of approximately 4-mm. The details of the impact tests are given in Table 2. This table indicates that all coupons were impacted with an impactor mass of 3.06 kg. Coupons A, B, K and L were impacted with 16.04 J, coupons C and D were impacted

Table 2
Impact tests conducted on 4-mm quasi-isotropic coupons.

Coupon	Avg. thickness (mm)	Mass (kg)	Height (cm)	Energy (J)	Impact velocity (m/s)	Momentum (Ns)	Damage size (in)	Ei (J)	% of Ei absorbed
A	4.18	3.059	53.462	16.042	2.884	8.822	1.317	12.724	77
B	4.19	3.059	53.462	16.042	2.881	8.811	1.271	12.692	75
C	4.07	3.059	35.121	10.539	2.283	6.984	0	7.9721	58
D	4.14	3.059	35.121	10.539	2.332	7.134	0	8.3188	64
E	4.21	3.059	44.877	13.466	2.575	7.877	0.32	10.142	55
F	4.17	3.059	44.877	13.466	2.739	8.378	0.33	11.474	58
G	4.05	3.059	49.169	14.754	2.815	8.612	0.42	12.122	55
H	4.08	3.059	49.169	14.754	2.787	8.526	1.33	11.882	77
I	4.25	3.059	39.023	11.710	2.423	7.411	0	8.9792	53
J	4.09	3.059	46.828	14.052	2.657	8.126	0.28	10.795	59
K	4.16	3.059	53.462	16.042	2.895	8.855	1.37	12.817	75
L	4.21	3.059	53.462	16.042	2.839	8.683	1.34	12.323	77

with 10.53 J, coupons E and F were impacted with 13.46 J, coupons G and H were impacted with 14.75 J, coupon I was impacted with 11.71 J and coupon J was impacted with 14.05 J. All the energies were incremented/decremented based on the previous tests and were estimated to try and obtain 1″ damage diameter in the 4-mm thick coupons. There seems to be a threshold phenomenon occurring where a very narrow range of energy exists where the damage diameter significantly increases with a small change in height for the same mass. This threshold phenomena could be attributed to the fact that some of the matrix cracks create the onset of larger than 1″ impact damage diameter. In coupons A, B, K and L with impactor energy of 16.04 J we were able to obtain approximately 1.3″ impact damage diameterwhich was closest to 1".

The force-time history of the impacts is given in Fig. 16. The load curve shows peaks at certain maximum load and is parabolic in shape. When the load curve is symmetric, its shape indicates that the impact energy is primarily deflected and little or no damage has occurred in the

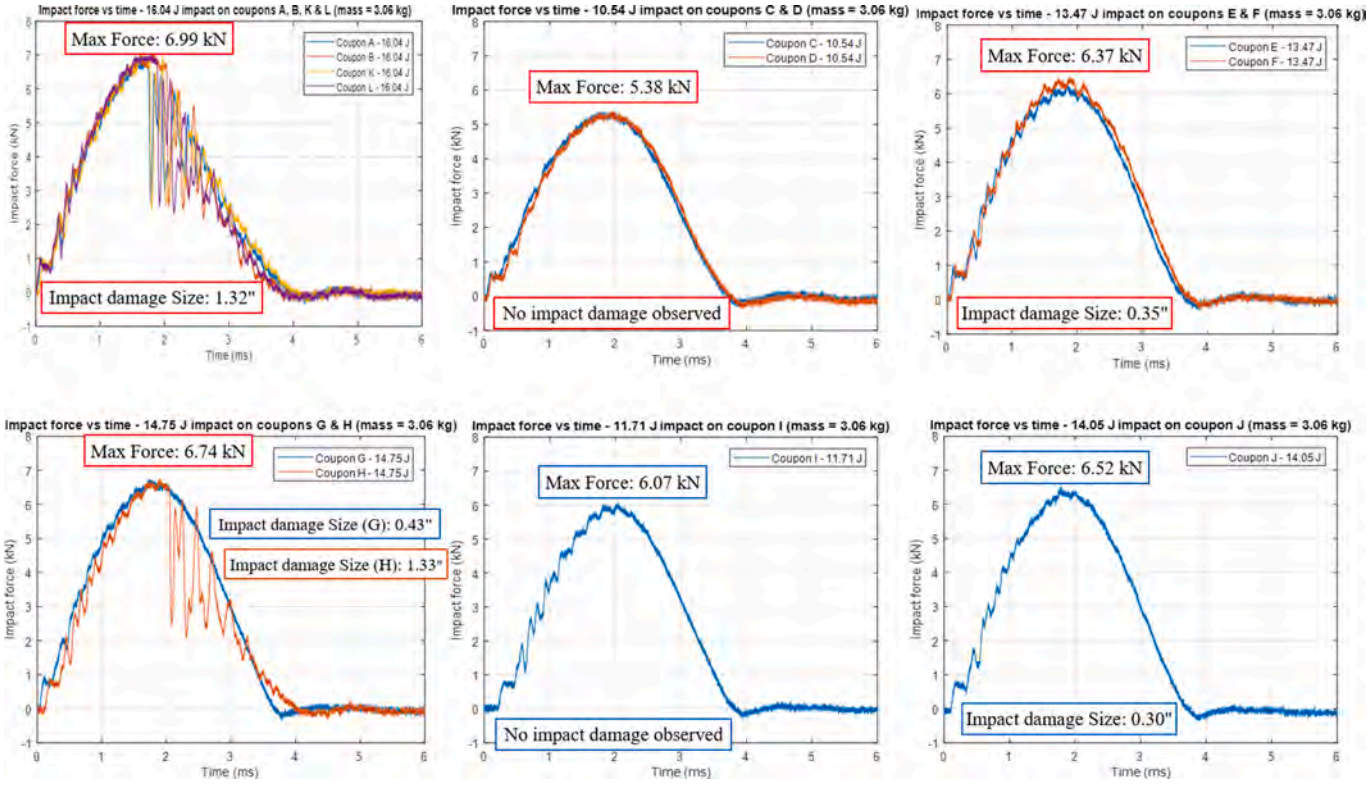

Fig. 16. Force-time history of $[-45/90/+45/0]_{4S}$ coupons.

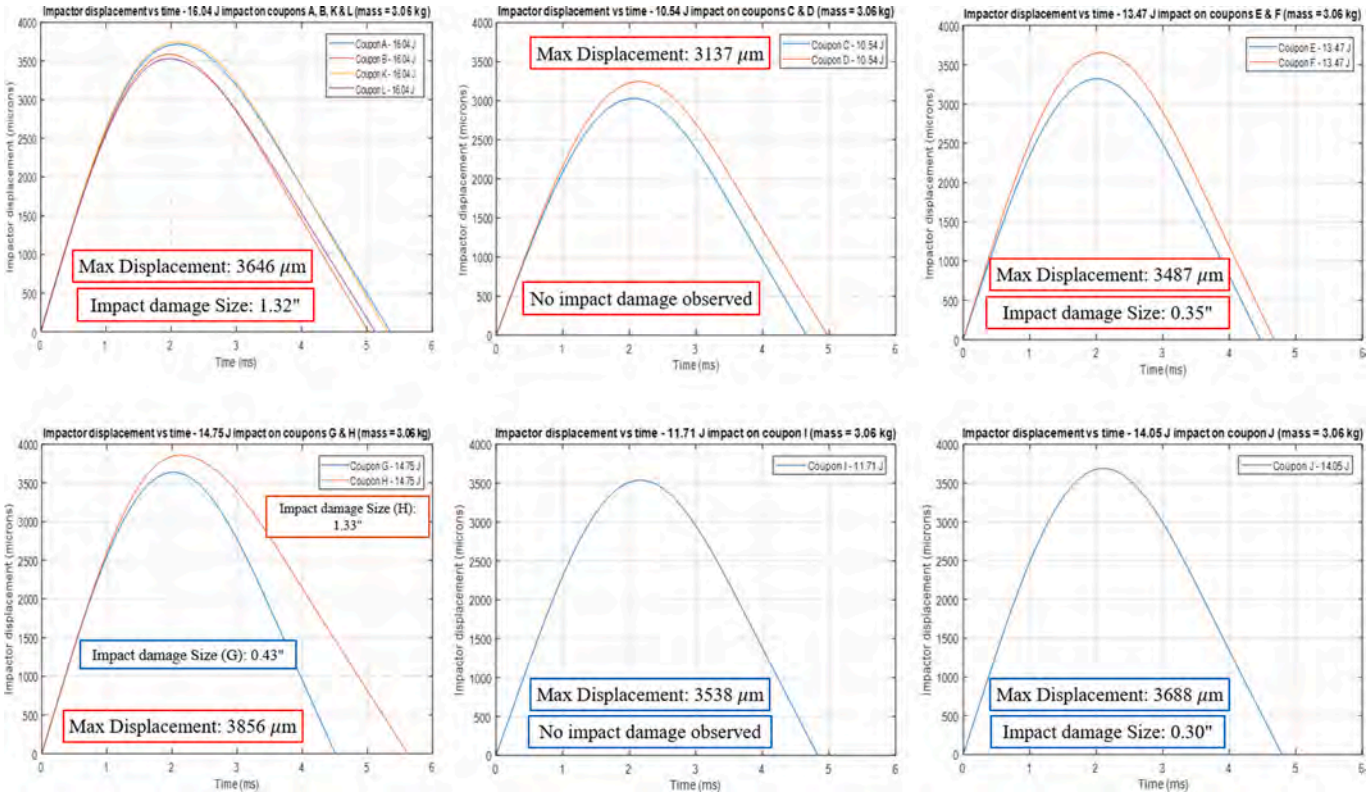

Fig. 17. Displacement-time history of $[-45/90/+45/0]_{4S}$ coupons.

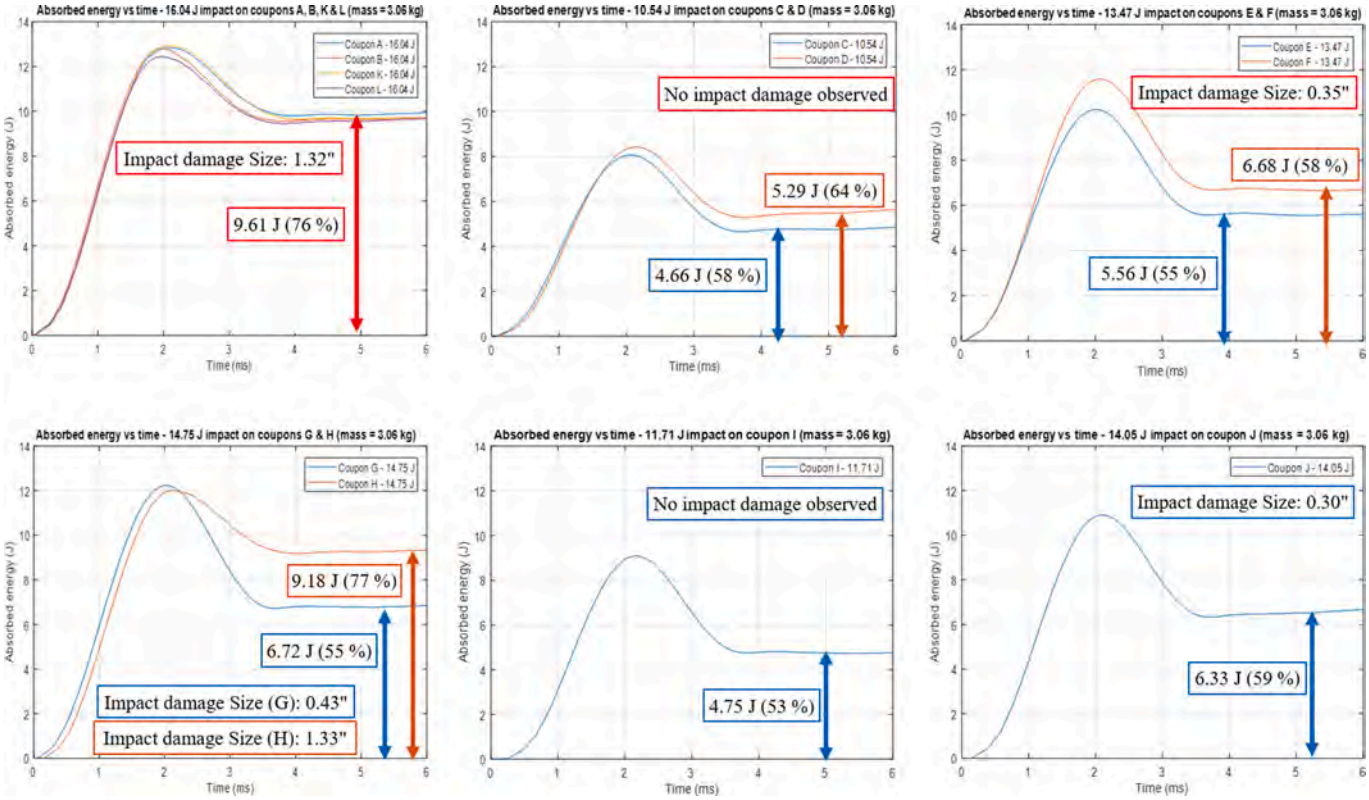

Fig. 18. Energy-time history of $[-45/90/+45/0]_{4S}$ coupons.

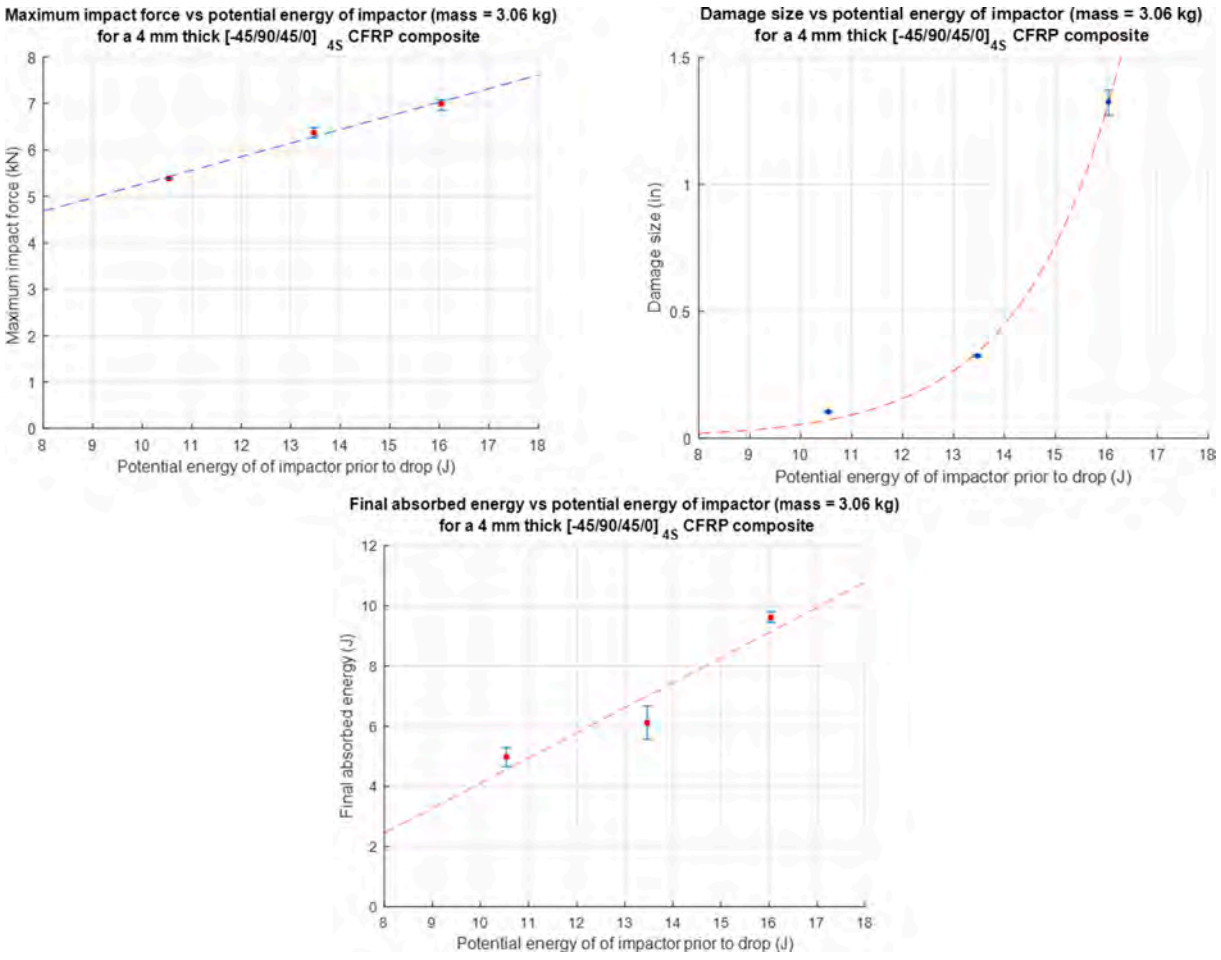

Fig. 19. Maximum impact force, impact damage size and absorbed enrgy of $[-45/90/+45/0]_{4S}$ coupons.

coupon. When there are irregularities in the parabolic shape of the load curve this indicates that the coupon has undergone extensive damage. These irregularities can be observed in force-time plots of coupons A, B, K and L and they seem to be very consistent. This can also be seen for coupon H which is clearly an outlier.

The velocity-time history of the impact events in the 4-mm coupons begins from being positive initially as the impactor is dropped towards the coupon then it becomes zero upon contacting the coupon and becomes negative as the impactor rebounds from the coupon and moves upwards. The displacement-time history of the coupons begins from zero and becomes maximum upon contacting with the impactor and then goes back to zero as the impactor is rebounded upwards as can be clearly observed in Fig. 17. We can clearly observe that the maximum displacement is obtained in coupon G for an impact energy of 14.75 J. Coupon H was an outlier as the same energy did not create any significant damage in coupon G. If we look at the force curves of coupons G and H we will observe that they have almost the same maximum force but their damage mechanisms are different due to their difference in strength which is anomalous.

The energy-time plots given in Fig. 18 is taken from the force-time curve through integration of the data. The energy-time history clearly is able to demonstrate the percentage of impact energy that is absorbed by the coupon to create the irreversible process of damage. For coupons A, B, K, L and G (outlier) where 1.3″ impact damage is formed, over 76% of the impact energy is absorbed by the coupons.

After performing these impact tests, the data obtained was further extrapolated to obtain a linear relationship between maximum impact force and potential energy of impactor. Similarly, a linear relationship was also obtained between the absorbed energy and potential energy of impactor. An exponential relationship was obtained between damage size and potential energy of impactor. These relationships are displayed in Fig. 19. From these impact experiments, we can also infer the effect of impact energy and impact momentum on damage size and penetration of damage across the thickness of these coupons as indicated in Fig. 20.

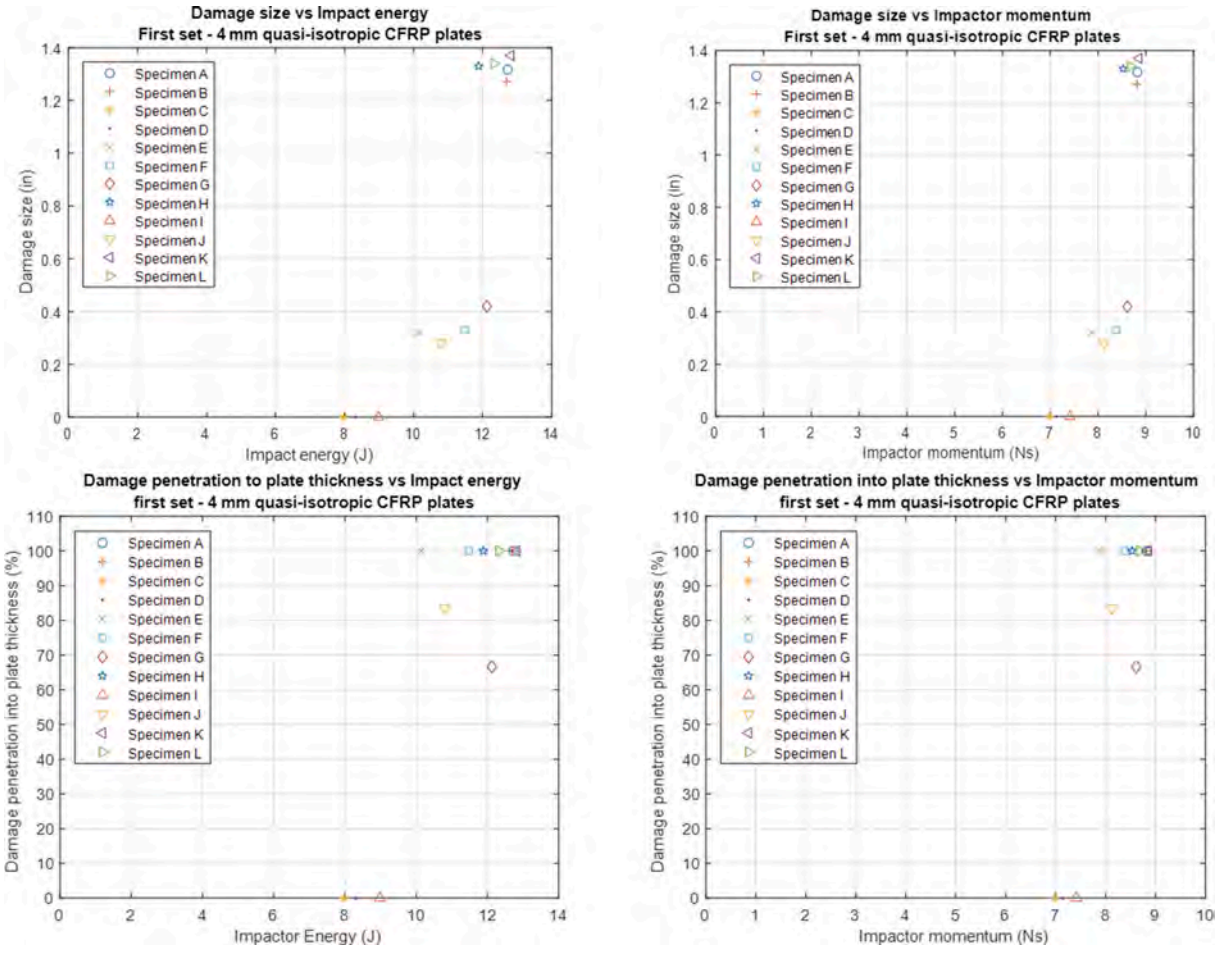

Fig. 20. Effect of impact energy and momentum on impact damage size in $[-45/90/+45/0]_{4S}$ coupons.

Here we can see a clustering effect where coupons impacted with the same energy have similar characteristics. Hence a mass, height and energy combination of the impactor was obtained to initiate a 1.3″ impact damage diameter in a $[-45/90/+45/0]_{4S}$ 4-mm thick quasi-isotropic coupon which was closest to 1″ damage.

Ultrasonic immersion tank scans were conducted to obtain the B-scan and C-scan images of the impact damage to observe its shape and size. From the B-scan, it can be seen that although, the center of the damage area undergoes permanent deformation similar to a dent, it does not have a delamination as a clear reflection from the center of the damage can be seen in the B-scan and it aligns with the bottom surface of the coupon. In addition, it can also be observed that the impact damage has propagated all the way through the thickness of the composite similar to the 2-mm coupon. From the C-scan image, we can clearly see that there is a small fiber pushout in the -45° fiber direction, and this can be seen by looking at the rear surface of the coupon as well. A quad plot of a representative coupon, displaying the force-time history, the energy time history, The B-scan and C-scan is observed in Fig. 21.

X-ray micro-CT imaging was conducted to obtain slices of the impact damage as it propagates from the top surface of the coupon to the bottom surface in a “rotating fan” phenomenon. The C-scan image (X–Y plane) at one of the bottom layers is displayed in Fig. 22 (a) along with the green dashed line and the blue dashed line which are the locations along which the B-scan images have been produced. The B-scan images of both the Z-X plane (Fig. 22 (b)) and the Y-Z plane (Fig. 22 (c)) can also be observed. From the B-scan images in can be observed that the center of the impact damage has a pyramidal shape and is composed of many matrix cracks and small delaminations in the form a staircase like transition.

Profilometry scans of the coupon were conducted similar to the previous section to observe the profile of the top and bottom surface after impact. The profilometry images are displayed in Fig. 23. Using the top surface scan, we were able to estimate that the dent depth is approximately 87 μm and using the bottom surface scan we were able to

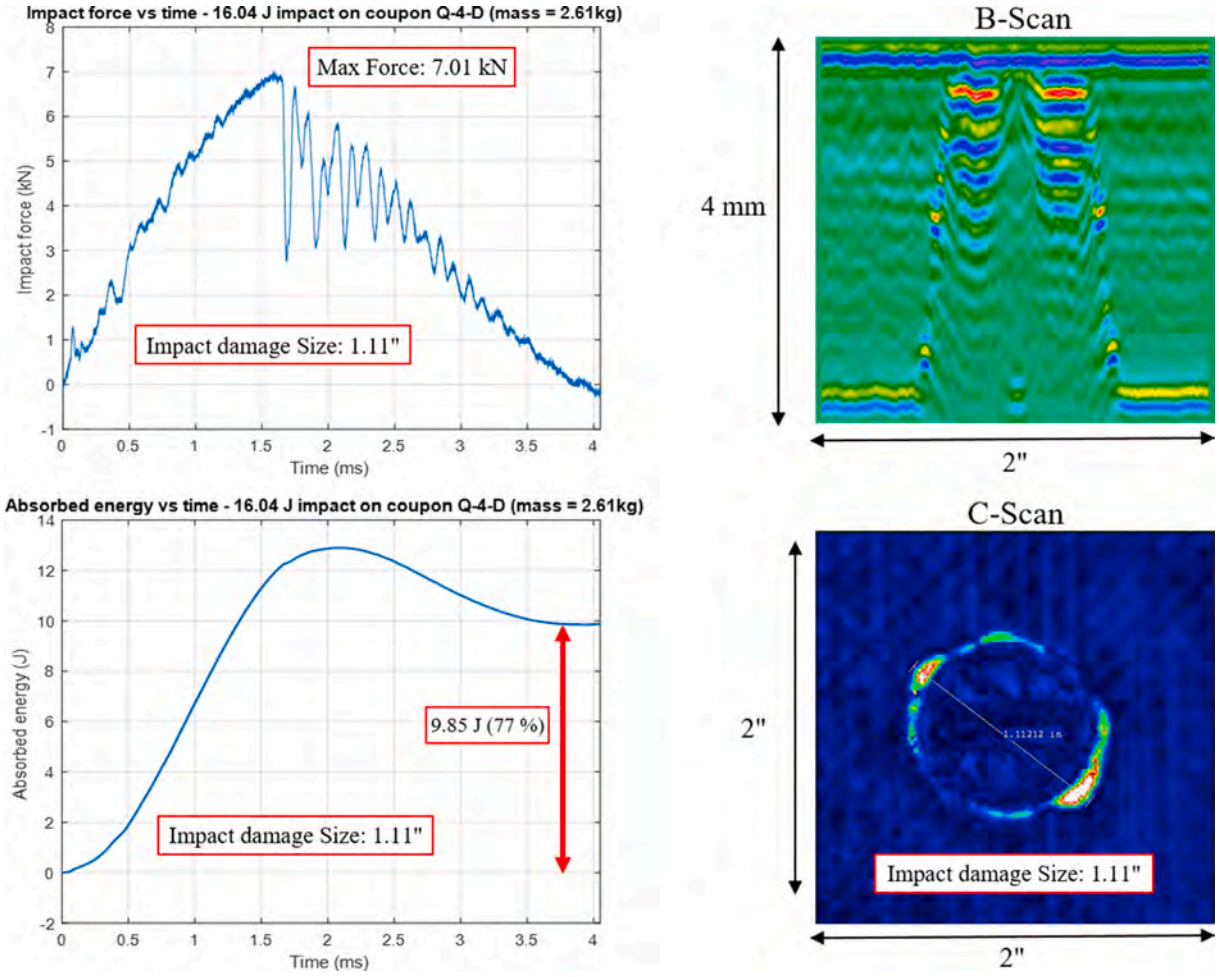

Fig. 21. Quad plot of 4-mm coupon with force-history, energy-history, B-scan and C-scan.

estimate the pushout height as 97 μm. As can be observed, the bottom surface of this coupon in Fig. 23 (b) has much lesser the irregularities when compared to the bottom surface of the 2-mm coupon in Fig. 23 (b). It is also interesting to observe that the dent profile seems a little flatter compared to the 2-mm coupon with a small dimple. The flatness in the surface profile is attributed to the additional 45° and −45° laminas in the 4-mm coupon which increases the flexural stiffness of the composite and therefore the coupon resist the bending due to impact.

5.3. Impact tests conducted on 6-mm quasi-isotropic coupons

Impact tests were conducted on various 6″ x 4” coupons having the stacking sequence of $[-45/90/+45/0]_{6S}$ which had thickness in the range of approximately 6-mm. The details of the impact tests are given in Table 3. This table indicates that coupon Q-6-A was impacted 6 times with different mass and heights, coupon Q-6-B and coupon Q-6-C were impacted twice, and coupons Q-6-D, Q-6-E and Q-6-F were impacted only once. Multiple impacts were conducted to try and obtain 1″ impact damage diameter in the 6-mm thick coupons. Despite numerous attempts there seems to be a threshold phenomenon occurring where the damage diameter significantly increases from less than 0.5″ to more than 1.7″ after multiple impacts. This threshold phenomena seems to be appearing in 6-mm coupons when they are subjected to multiple impact. The first impact creates a small size impact damage diameter of less than 0.5″ along with some matrix cracks. Upon the second impact on the same coupon, these matrix cracks widen uncontrollably and lead to the onset of an impact damage diameter of more than 1.7".

The force-time history of the impacts are given in Fig. 24, Fig. 25 and

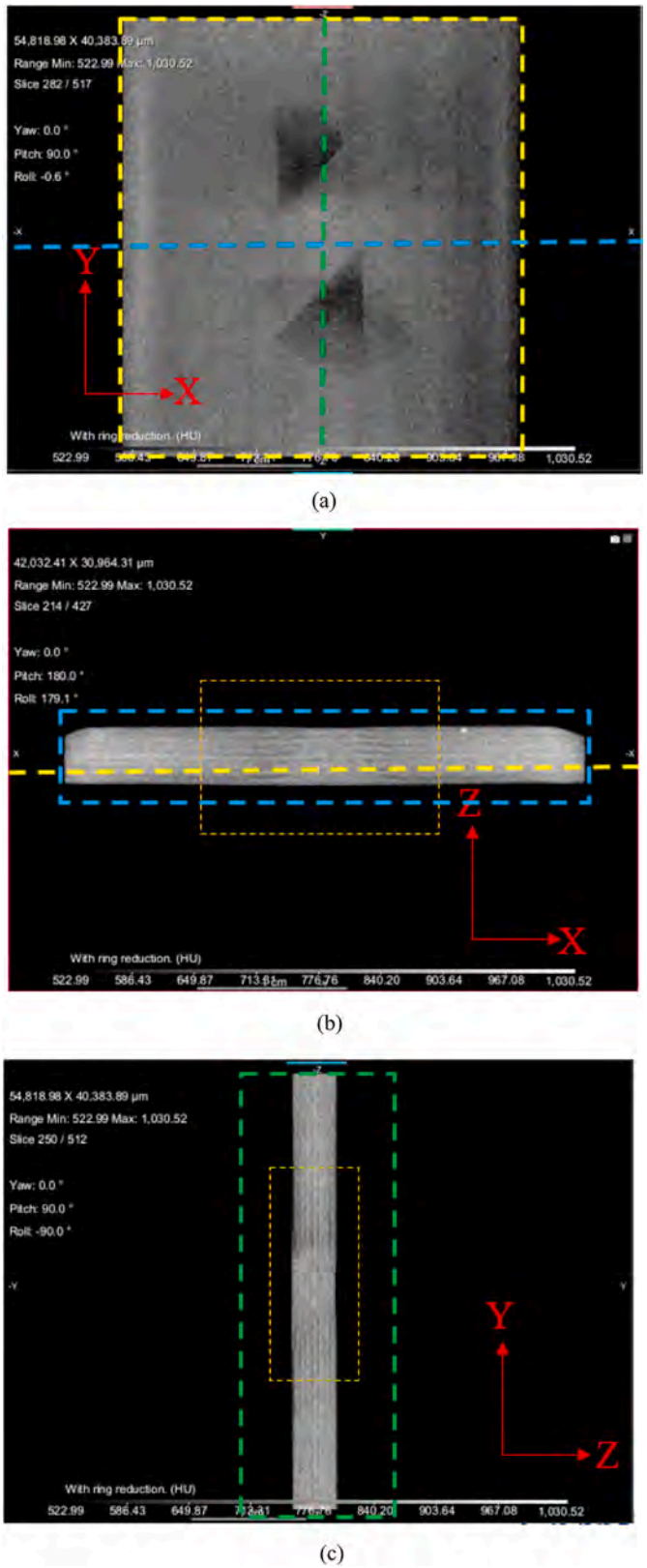

Fig. 22. X-ray micro-CT of 4 mm coupon with 1″ impact damage.

Fig. 26. The force-time curve shows peaks at certain maximum load and is parabolic in shape. When the load curve is symmetric, its shape indicates that the impact energy is primarily deflected and little or no damage has occurred in the coupon. When there are irregularities in the parabolic shape of the load curve this indicates that the coupon has

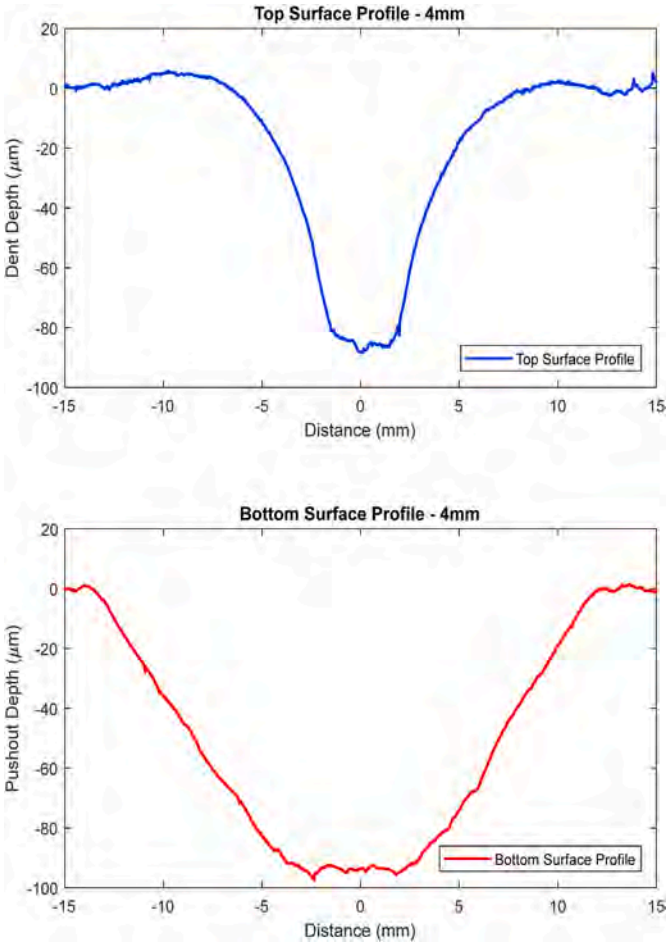

Fig. 23. Profilometry scans of 4-mm coupon: (a) Top surface; (b) Bottom surface.

undergone extensive damage. These irregularities can be observed in all coupons at the final impact where the damage significantly increases in the coupons.

The velocity-time history of the impact events in the 6-mm coupons is similar to the behavior described for the 2-mm and 4-mm coupons. The displacement-time history of the coupons also has a similar trend as displayed by previous coupons and can be clearly observed in Fig. 27, Fig. 28 and Fig. 29.

The energy-time plots given in Fig. 30, Fig. 31 and Fig. 32 is taken from the force-time curve through integration of the data. The energy-time history clearly is able to demonstrate the percentage of impact energy that is absorbed by the coupon to create the irreversible process of damage. Similar to the 4-mm plate, there seems to be a threshold phenomenon occurring where if the absorbed energy is more than 79%, it creates a impact damage diameter of 1.7″ or more in the 6-mm plate.

From these impact experiments, we can also infer the effect of impact energy and impact momentum on impact damage size and penetration of damage across the thickness of these coupons as indicated in Fig. 33. Hence a mass, height and energy combination of the impactor was obtained to initiate a 1.8″ or greater size damage in a $[-45/90/+45/0]_{6S}$ 6-mm thick quasi-isotropic coupon.

Ultrasonic immersion tank scans were conducted to obtain the B-scan and C-scan images of the impact damage to observe its shape and size similar to the previous two sections. From the B-scan, it can be observed that the impact damage has not propagated all the way through the thickness of the composite coupon which did occur in the case of the 2-mm coupon and the 4-mm coupon. From the C-scan image, we can clearly see that the damage diameter is 1.79″ which was the

Table 3
Impact tests conducted on 6-mm quasi-isotropic coupons.

Coupon	Avg. thickness (mm)	Mass (kg)	Height (cm)	Energy (J)	Impact velocity (m/s)	Momentum (Ns)	Damage size (in)	Ei (J)	% of Ei absorbed
Q-6-A	6.29	3.059	53.462	16.042	2.980	9.12	0	13.619	65
Q-6-A	6.29	3.059	78.047	23.419	3.630	11.10	0.25	20.122	61
Q-6-A	6.29	5.406	20.556	10.901	2.060	11.14	0.29	11.530	62
Q-6-A	6.29	5.406	41.112	21.801	2.850	15.41	0.44	21.970	59
Q-6-A	6.29	7.628	14.196	10.622	1.770	13.50	0.48	11.998	61
Q-6-A	6.29	7.628	28.391	21.244	2.470	18.84	1.91	23.323	76
Q-6-B	6.32	3.059	58.535	17.565	3.060	9.36	0	14.350	67
Q-6-B	6.32	7.628	28.391	21.244	2.530	19.30	1.9	24.394	82
Q-6-C	6.28	6.566	24.988	16.095	2.340	15.36	0.3	18.040	57
Q-6-C	6.28	6.566	33.318	21.460	2.660	17.46	1.8	23.191	78
Q-6-D	6.27	5.406	61.668	32.702	3.540	19.14	2.2	33.848	76
Q-6-E	6.18	5.406	51.390	27.251	3.320	17.95	1.88	29.802	82
Q-6-F	6.25	5.406	41.112	21.801	2.870	15.51	1.79	22.356	79

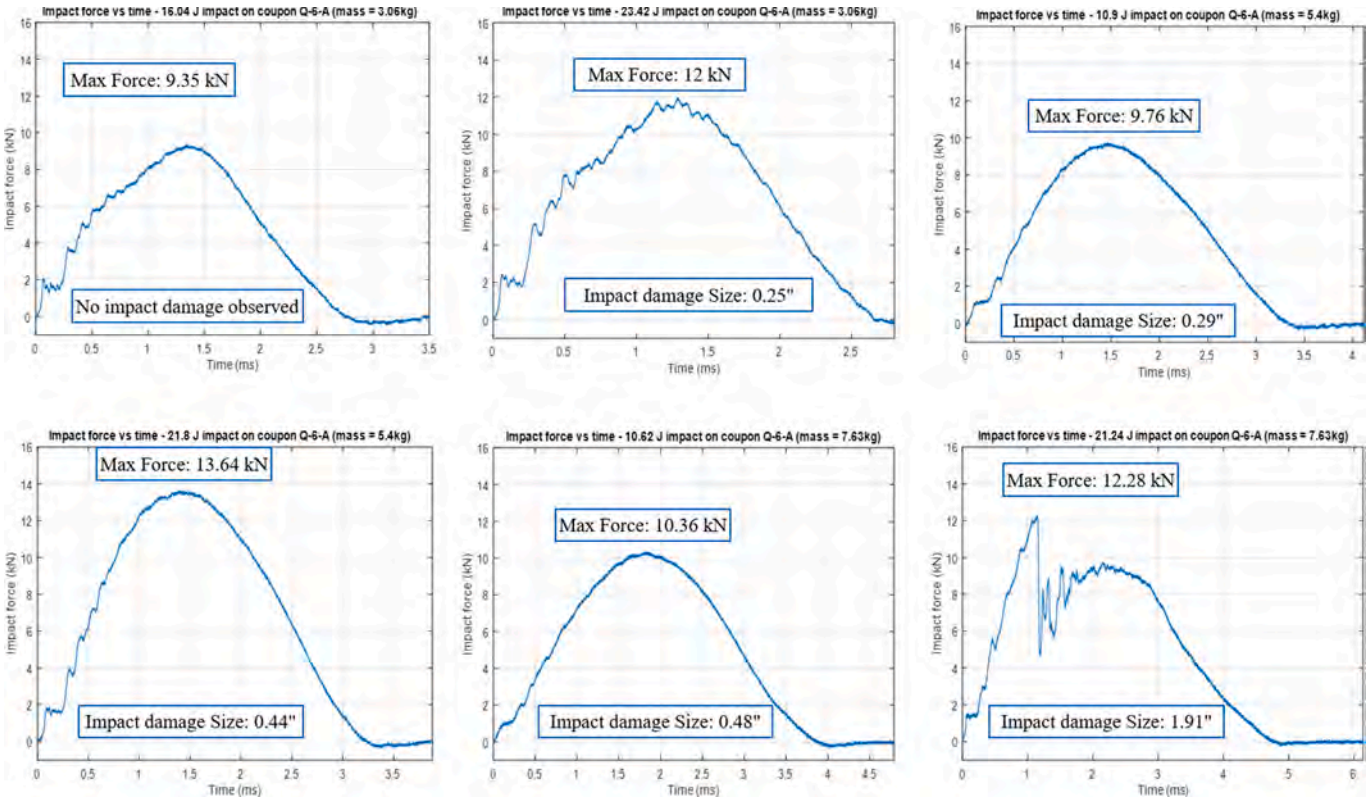

Fig. 24. Force-time history of $[-45/90/+45/0]_{6S}$ coupon Q-6-A for multiple impacts.

damage diameter that was closest to 1″ that could be obtained. It can also be observed from the C-scan that the maximum damage is now in the 90° fiber direction as opposed to the −45° fiber direction in the 2-mm and 4-mm coupons because the damage had propagated through the thickness for the 2-mm and 4-mm coupon and has not propagated through the thickness for the case of the 6-mm coupon. A quad plot of a representative coupon, displaying the force-time history, the energy time history, The B-scan and C-scan is observed in Fig. 34.

X-ray micro-CT imaging was conducted to obtain slices of the impact damage as it propagates from the top surface of the coupon to the bottom surface in a "rotating fan" phenomenon. The C-scan image (X–Y plane) at one of the bottom layers is displayed in Fig. 35 (a) along with the green dashed line and the blue dashed line which are the locations along which the B-scan images have been produced. From the C-scan image, we can clearly observe a large delamination on the right hand side of the impacted region. The B-scan images of both the Z-X plane (Fig. 35 (b)) and the Y-Z plane (Fig. 35 (c)) can also be observed. From the B-scan images in can be observed that the center of the impact

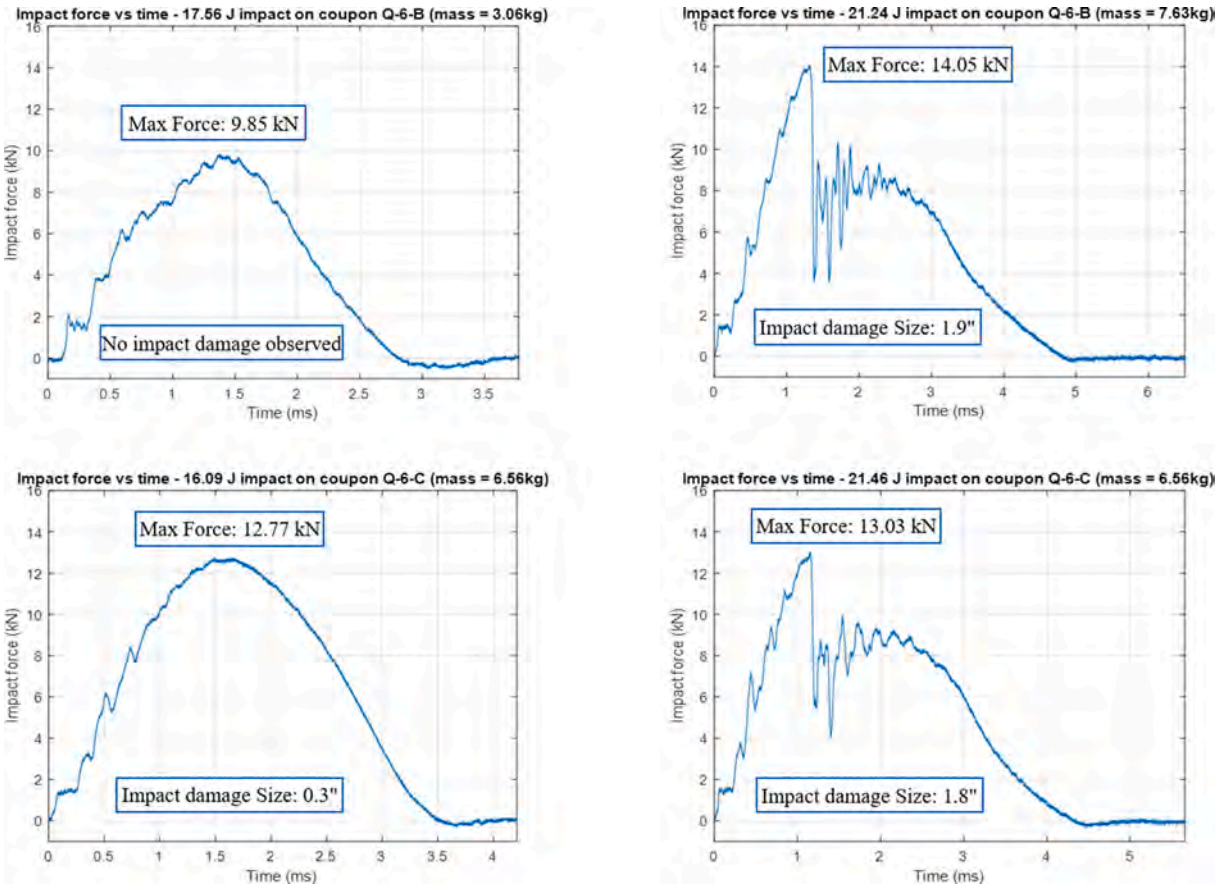

Fig. 25. Force-time history of $[-45/90/+45/0]_{6S}$ coupons Q-6-B and Q-6-C for multiple impacts.

damage has a pyramidal shape which is more sporadic than the scenarios of the 2-mm and 4-m coupons and is composed of many matrix cracks and small delaminations in the form a staircase like transition.

Profilometry scans of the coupon were conducted similar to the previous section to observe the profile of the top and bottom surface after impact. The profilometry images are displayed in Fig. 36. Using the top surface scan we were able to estimate that the dent depth is approximately 119 μm and using the bottom surface scan we were able to estimate the pushout height as 93 μm. As can be observed, the bottom surface of this coupon in Fig. 36 (b) does not cover the entire damage since it is greater than 1″ and the scanning area is also limited by the bounds of the surface profiler when compared to the bottom surface of the 2-mm coupon in Fig. 15 (b) and 4-mm coupon in Fig. 23 (b). It is also interesting to observe that the dent profile seems flatter in Fig. 36 (a) compared to the 2-mm and 4-mm coupon with a small dimple. The flatness in the surface profile is attributed to the additional 45° and −45° laminas in the 6-mm coupon compared to the 2-mm and 4-mm coupons which increases the flexural stiffness of the composite and therefore the coupon resist the bending due to impact. This is an interesting observation and has not been reported before in literature. From this observation, we can assume that as the thickness of the impacted coupons increases, the profile of the impacted surface becomes flatter and less hemispherical.

5.4. *MODIFIED EXPERIMENTAL SETUP FOR DROP WEIGHT IMPACT TESTING*

After having some difficulties in obtaining the mass, height and energy combination to obtain 1″ impact damage diameter in the 4-mm and 6-mm thick coupons, it was assumed that due to the thickness of the coupons being more than 2-mm, the in-plane dimensions (aspect ratio) needed to be increased so that the coupon could be bent more in flexure upon impact. Since the ASTM D7136 fixture has maximum in-plane dimensions of 12″ × 6″, the coupon dimensions will be changed from 6″ × 4″ to 12″ × 6" (since that is the in-plane dimension of the fixture). Two rectangular frames have been constructed that will hold the larger coupon and be clamped to the D7136 fixture to conduct impact tests on the same drop tower. These tests will not conform to ASTM D7136 standards. The modified experimental setup is displayed in Fig. 37. These tests will be conducted in the future to try and obtain close to 1″ impact damage diameter in thick composite coupons. Guided-wave

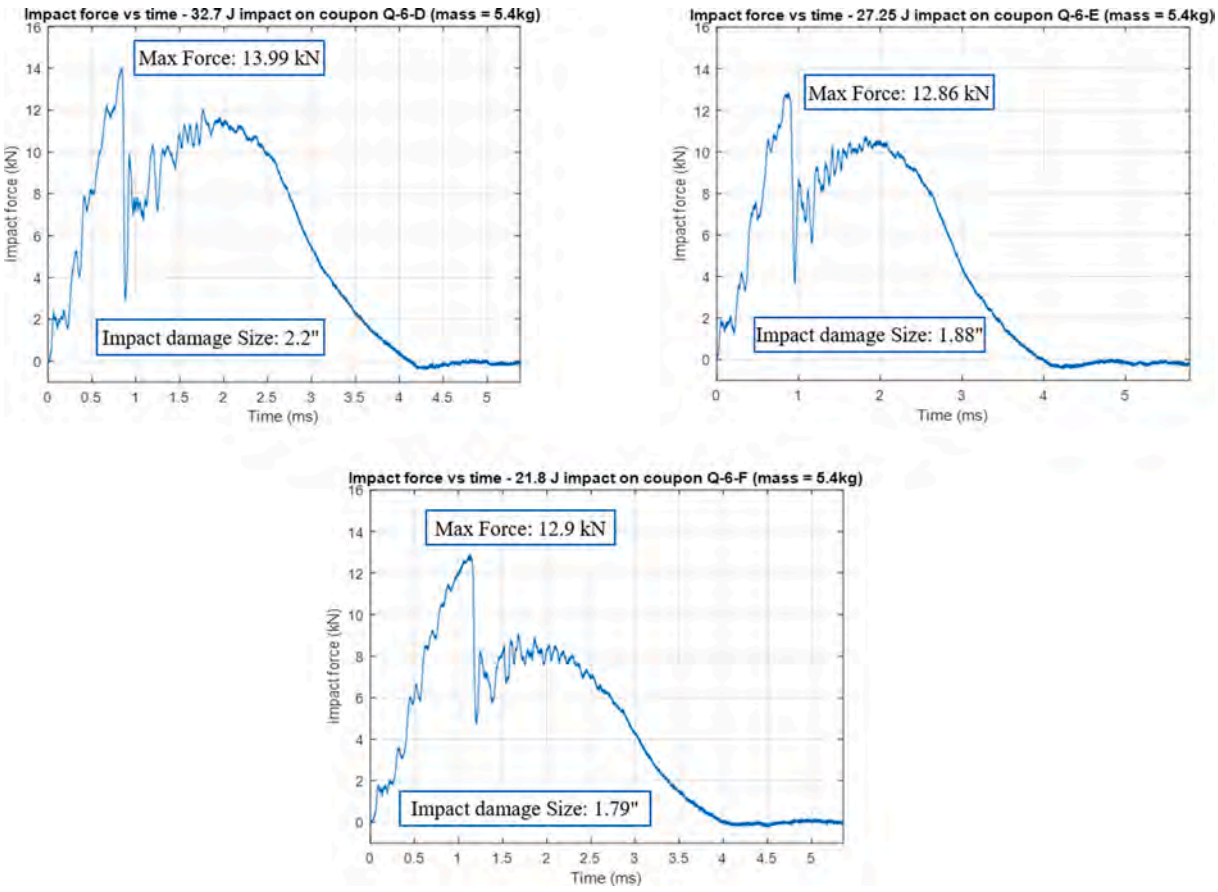

Fig. 26. Force-time history of $[-45/90/+45/0]_{6S}$ coupons Q-6-D, Q-6-E and Q-6-F.

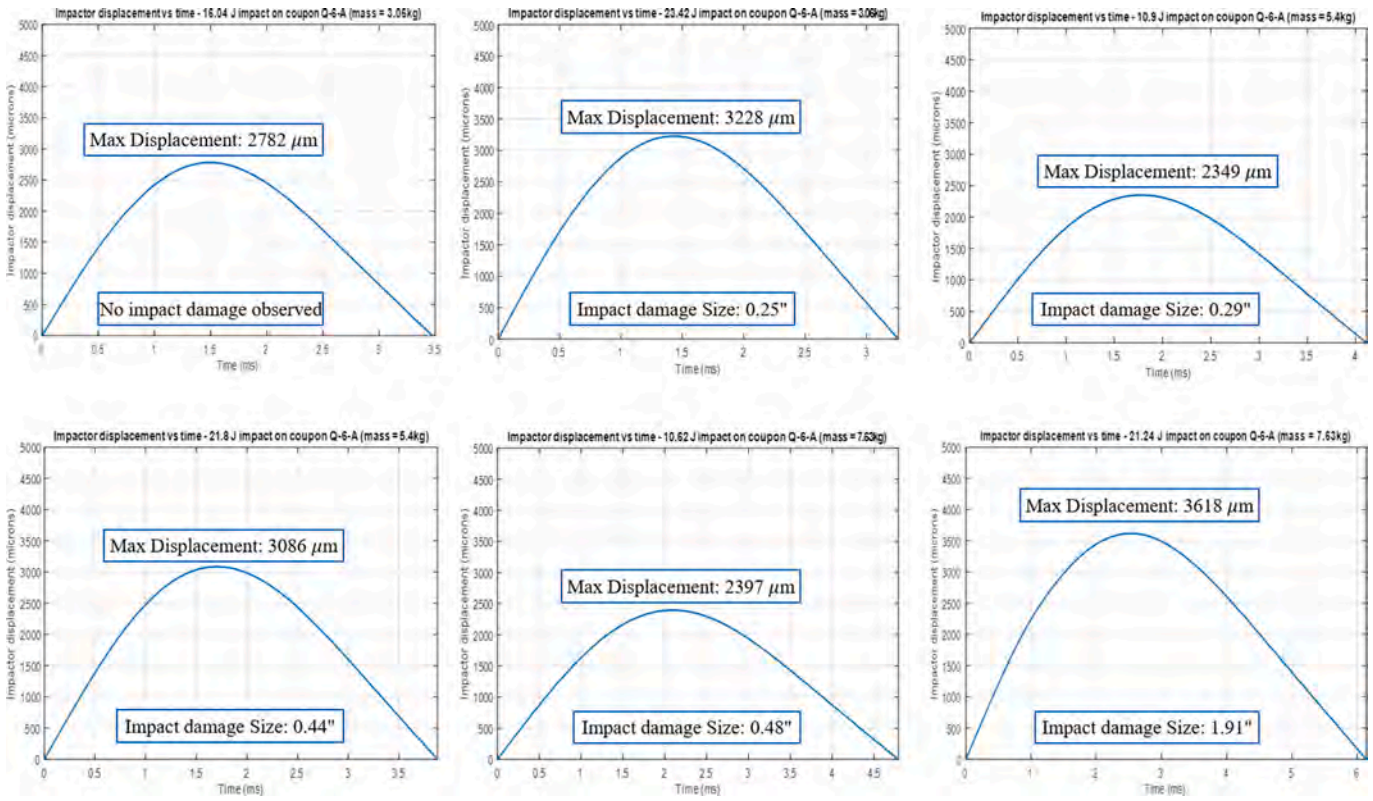

Fig. 27. Displacement-time history of $[-45/90/+45/0]_{6S}$ coupon Q-6-A for multiple impacts.

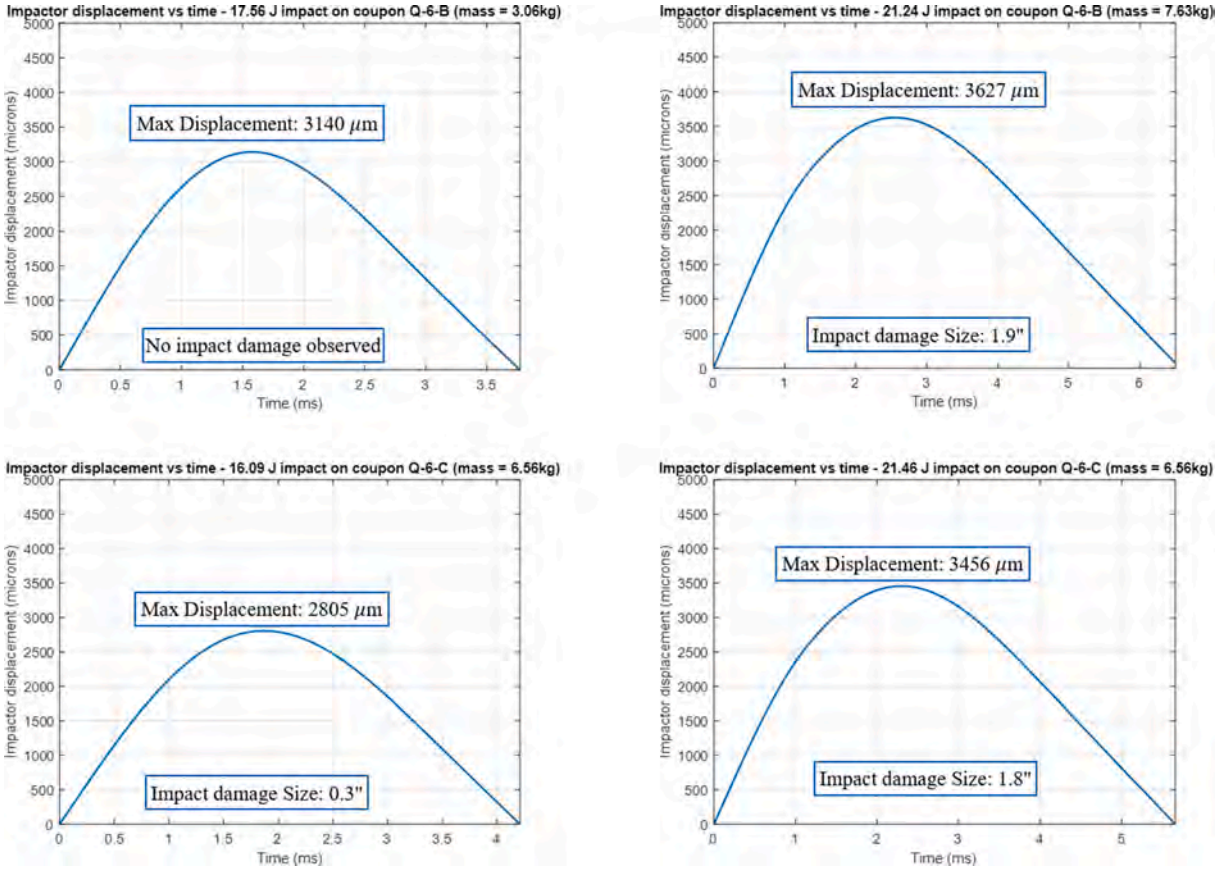

Fig. 28. Displacement-time history of $[-45/90/+45/0]_{6S}$ coupons Q-6-B and Q-6-C for multiple impacts.

based methods will also be explored to detect impact damage of different sizes and distinguish impact damage from a simulated delamination. The use of X-ray computed tomography will also be explored as an impact damage detection technique in addition to the aforementioned methods.

5.5. Impact tests conducted on 12″ × 6″, 6-mm quasi-isotropic coupons

Using the modified experimental setup, impact tests were conducted on various 12″ × 6″ coupons having the stacking sequence of $[-45/90/+45/0]_{6S}$ which had thickness in the range of approximately 6-mm. The details of the impact tests are given in Table 4. In Section 5.3 the impact tests conducted on 6″ × 4″, 6-mm thick coupons designated as Q-6-A, Q-6-B, etc. were discussed. In this section, the 12″ × 6″, 6-mm thick coupons will be designated as QL6A, QL6B, etc. The data in Table 4 indicates that coupon QL6A, QL6B and QL6C were each impacted 2 times with the same mass but different heights to try and obtain close to 1″ impact damage diameter. Coupon QL6D was impacted only once. Double impacts were conducted to try and obtain 1″ impact damage diameter in the 6-mm thick coupons. Despite numerous attempts there seems to be a threshold phenomenon occurring where the damage diameter significantly increases from less than 0.45″ to more than 2″ after double impacts. A similar threshold phenomenon was observed in the 6-mm coupons of having a standard size of 6″x 4".

The force-time histories of the double impacts conducted on coupons QL6A, QL6B and QL6C are displayed in Fig. 38. The force-time curves show peaks at certain maximum load and are parabolic in shape. When the load curve is symmetric, its shape indicates that the impact energy is primarily deflected and little or no damage has occurred in the coupon. When there are irregularities in the parabolic shape of the load curve this indicates that the coupon has undergone extensive damage. The first impacts as indicated by the plots on the left hand side show little or no

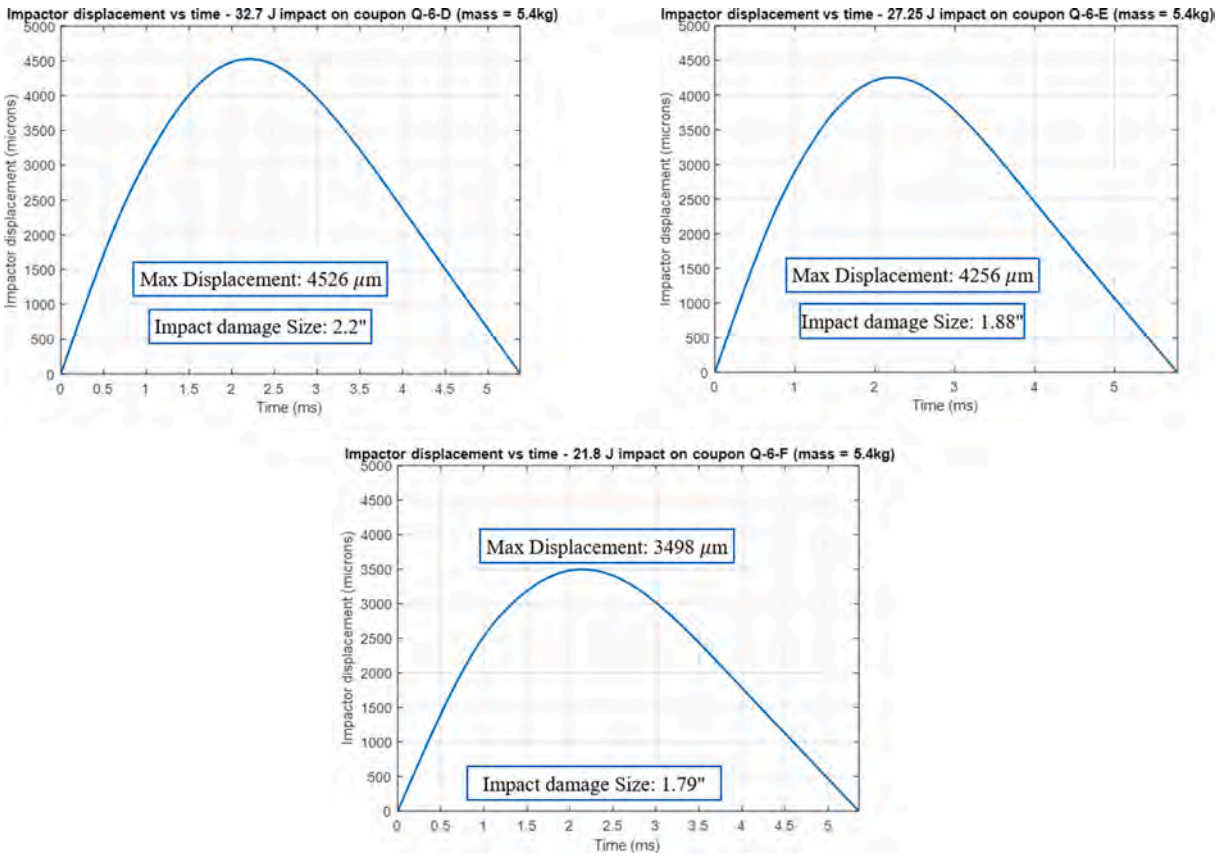

Fig. 29. Displacement-time history of $[-45/90/+45/0]_{6S}$ coupons Q-6-D, Q-6-E and Q-6-F.

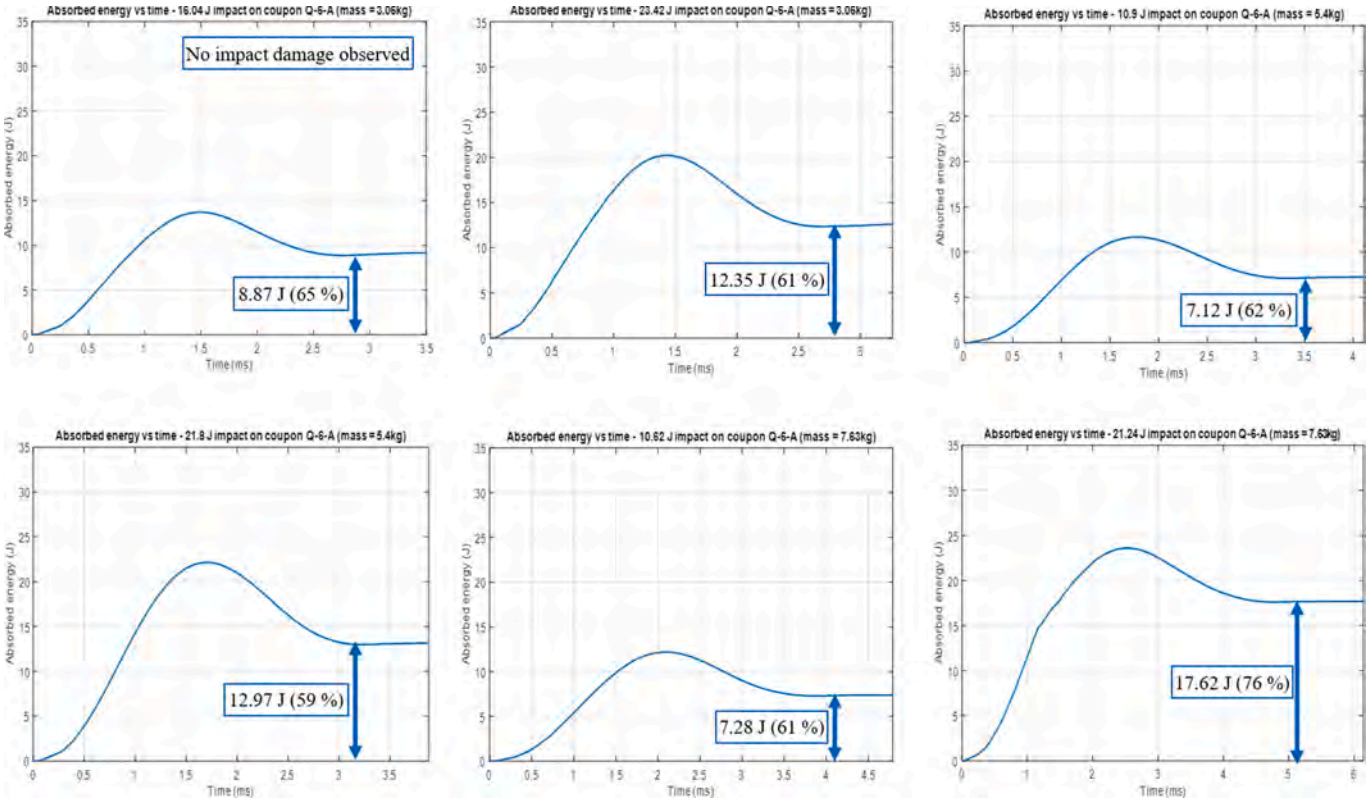

Fig. 30. Energy-time history of $[-45/90/+45/0]_{6S}$ coupon Q-6-A for multiple impacts.

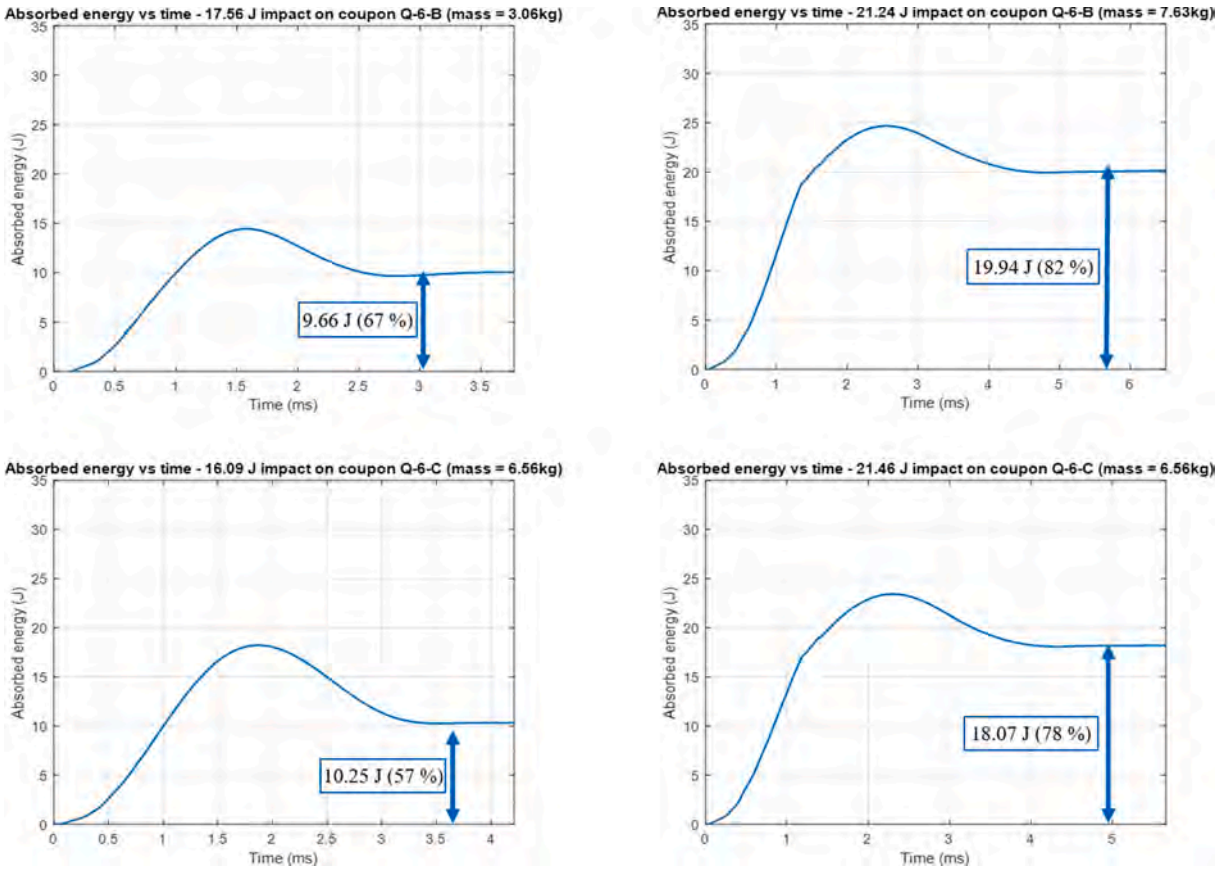

Fig. 31. Energy-time history of $[-45/90/+45/0]_{6S}$ coupons Q-6-B and Q-6-C for multiple impacts.

irregularities indicating that there was little to no internal damage in the coupons. Some irregularities can clearly be observed in the three coupons at the second impact where the damage significantly increases in the coupons. For coupon QL6D, it can be observed from its force-time history in Fig. 39 that even with the impact energy comparable to the second impact on coupon QL6C which created 2″ impact damage diameter in it, there is only a damage of 0.37″ created in coupon QL6D which indicates the threshold phenomena described earlier.

The velocity-time history of the impact events in these 6-mm coupons is similar to the behavior described in the previous sections. The displacement-time histories of the double impacts conducted on coupons QL6A, QL6B and QL6C are displayed in Fig. 40 where the second impact clearly create a larger displacement as compared to the first impacts. The displacement-time history of coupon QL6D is displayed in Fig. 41 and indicates a displacement value comparable to the second impacts of the previous coupons but crates a fraction of the impact damage size.

The energy-time plots of the double impacts conducted on coupons QL6A, QL6B and QL6C are displayed in Fig. 42 and clearly able to demonstrate the percentage of impact energy that is absorbed by the coupon to create the irreversible process of damage. For the first impact we can observe that the absorbed impact energy is only 50% of the impact energy and for the second impact more than 68% of the impact energy is absorbed by the coupons. The energy-time history of coupon QL6D is displayed in Fig. 43. In this coupon although the impact energy is comparable to the second impact conducted on coupon QL6C, it only absorbs 50% of the impact energy which is similar to the first impacts on the previous coupons. Similar to the previous sections, there seems to be a threshold phenomenon occurring where if the absorbed energy is more than 68%, it creates a impact damage diameter of 2″ or more in the 12” x 6″, 6-mm coupons.

From these impact experiments, we can also infer the effect of impact energy and impact momentum on impact damage size and penetration of damage across the thickness of these coupons as indicated in Fig. 44. In these plots, the first impacts and the second impacts have the numbers “1” and “2” before the symbols indicating the impacts. From these impact experiments, a mass, height and energy combination of the impactor was obtained to initiate a 2″ or greater size impact damage in a $[-45/90/+45/0]_{6S}$ 6-mm thick quasi-isotropic coupon having a coupon size of 12″ × 6".

Ultrasonic immersion tank scans were conducted to obtain the B-scan and C-scan images of the impact damage to observe its shape and size similar to the previous three sections. From the B-scan, it can be observed that the impact damage has not propagated all the way

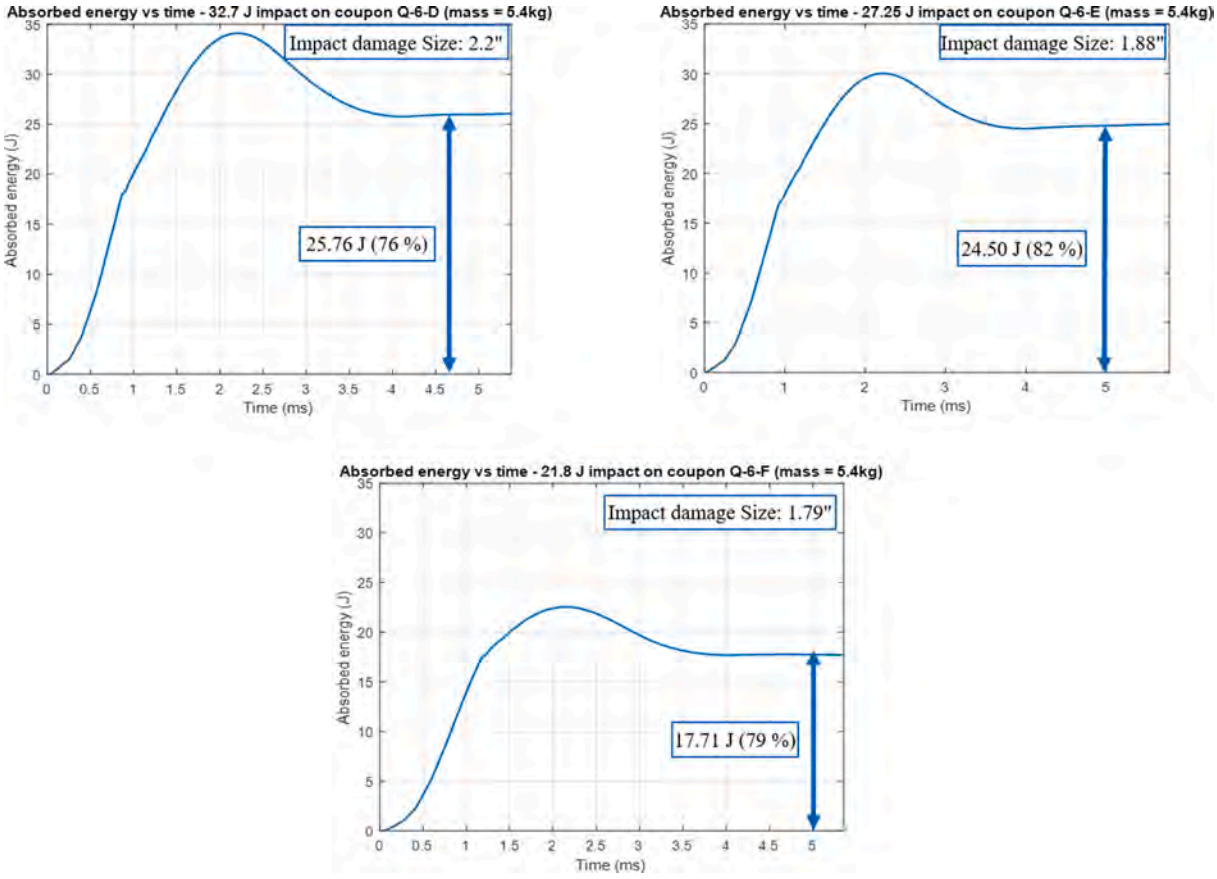

Fig. 32. Energy-time history of $[-45/90/+45/0]_{6S}$ coupons Q-6-D, Q-6-E and Q-6-F.

through the thickness of the composite coupon which is similar to the previous section where the 6″ × 4″, 6-mm coupons was examined. This phenomenon did occur in the case of the 2-mm coupon and the 4-mm coupon. From the C-scan image, we can clearly see that the damage diameter is approximately 2″ which was the damage diameter that was closest to 1″ that could be obtained. It can also be observed from the C-scan that the maximum damage is now in the −45° fiber direction even though the damage has not propagated through the thickness of the 6-mm coupon. A quad plot of a representative coupon QL6B, displaying the force-time history, the energy time history, The B-scan and C-scan is observed in Fig. 45.

6. Summary, conclusions and future work

6.1. Summary

In this paper, drop weight impact experiments were conducted on quasi-isotropic CFRP composite coupons of different thicknesses ranging from 2-mm to 6-mm conforming to the ASTM D7136 standard. The purpose of the impact experiments was to find the mass-height combination to obtain approximately 1″ impact damage diameter. Force-time history, displacement-time history and energy-time history plots were obtained for each coupon that was tested using different mass-height combinations. Ultrasonic immersion tank scans and X-ray micro-CT scans were used to visualize the size of damage and profilometry scans were used to evaluate the dent depth and the pushout height of the top and bottom surfaces of the impacted coupons respectively. Representative coupons from each thickness that produced closest to 1″ impact damage diameter were represented in a quad plot with the force-time history, energy-time history, B-scan image and C-scan image.

6.2. Conclusions

From the impact experiments, it was observed that the mass-height combination to obtain controlled 1″ impact damage diameter can be obtained in relatively thin quasi-isotropic composite coupons (2–4 mm) and becomes much harder to obtain in thick quasi-isotropic composite coupons. (5–6 mm). For thicker composite coupons there seemed to be a

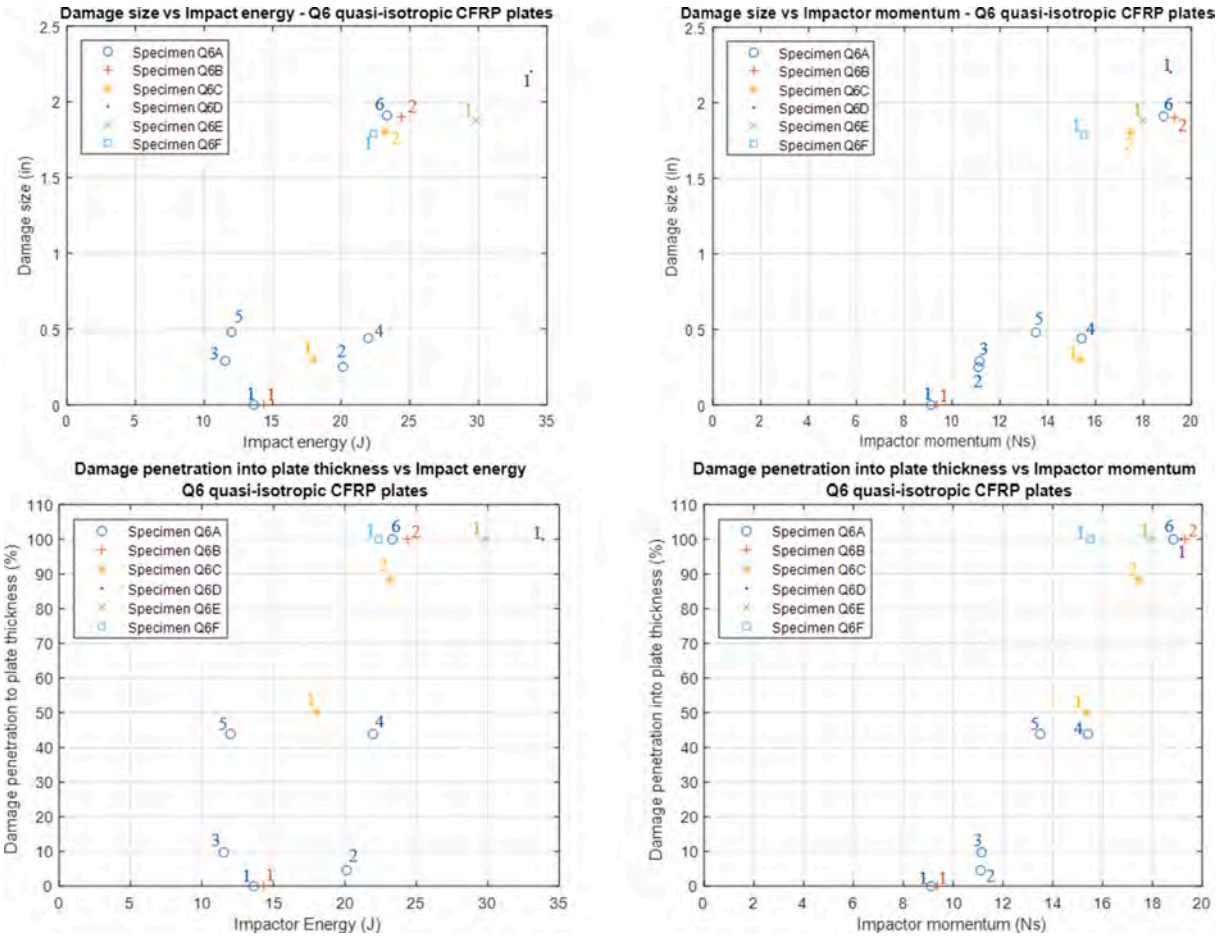

Fig. 33. Effect of impact energy and momentum on impact damage size in $[-45/90/+45/0]_{6S}$ coupons.

threshold phenomenon occurring where similar mass-height combination would produce small damage diameter in one coupon and large damage diameter in another coupon. From the profilometry scans, it was observed that as the thickness of the composite coupon being tested is increased, the dent of impact becomes flatter even though the tip of the tup has a hemispherical shape in accordance with the ASTM D7136 standard. For thin coupons, the hemispherical shape of the tup was recovered in the hemispherical shape of the indentation. However, for thicker coupons, the indentation developed a flat bottom in spite of the fact that the tip of the tup was hemispherical. This phenomenon may be attributed to the microscale failure process taking place in the composite under the tip of the impactor tup. In thinner composites, this process seems to be different from the process taking place in thicker composites. This can also be attributed to the fact that as the number of 45° and −45° laminas is increased in the composite there is an increase in the flexural stiffness of the composite and therefore the coupon resist the bending due to impact. To the best of our knowledge, this observation has not been previously reported in the literature. Impact tests conducted on CFRP coupons with controlled damage size would serve in the future for validation of structural health monitoring (SHM) and nondestructive evaluation (NDE) damage detection methodology.

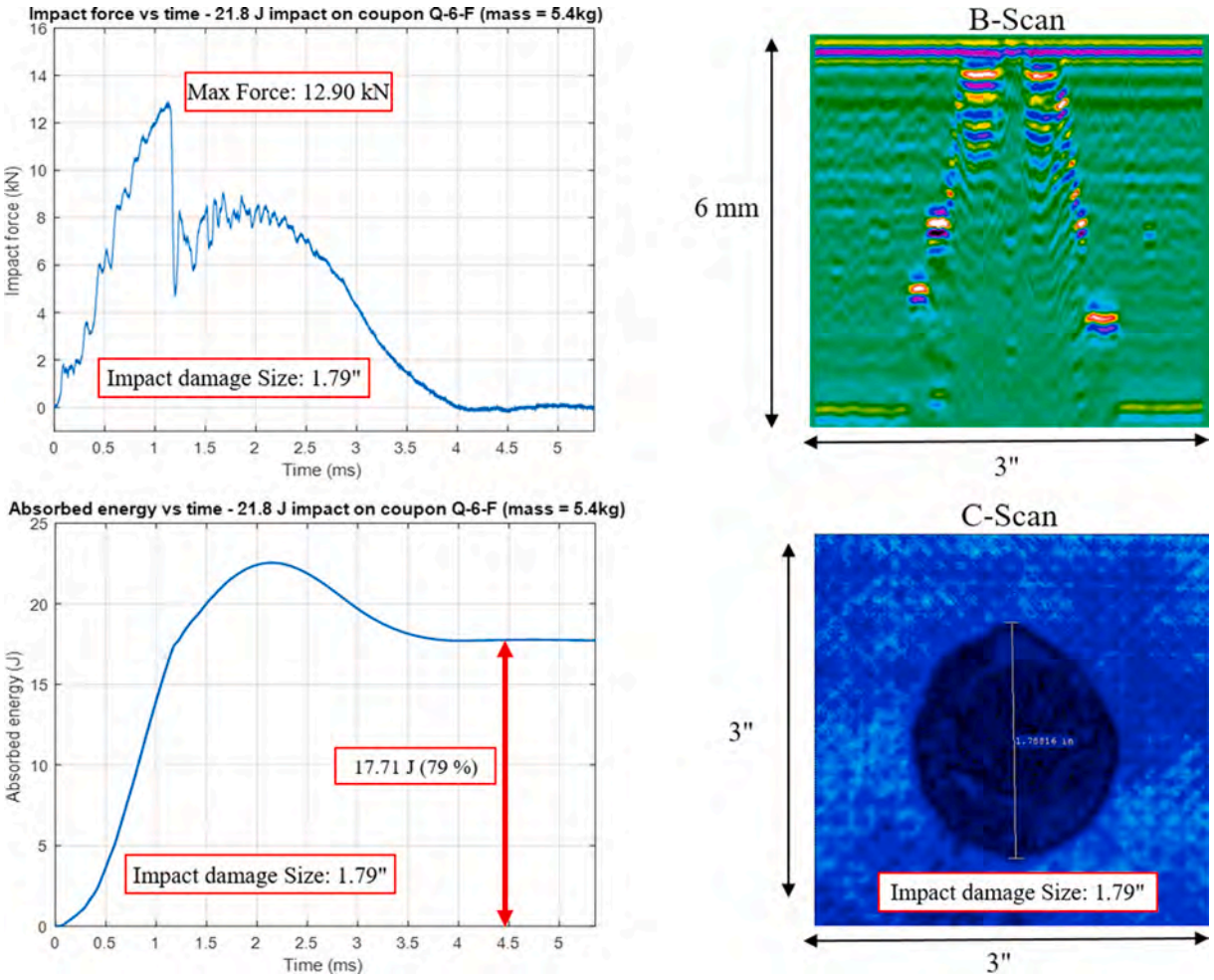

Fig. 34. Quad plot of 6-mm coupon with force-history, energy-history, B-scan and C-scan.

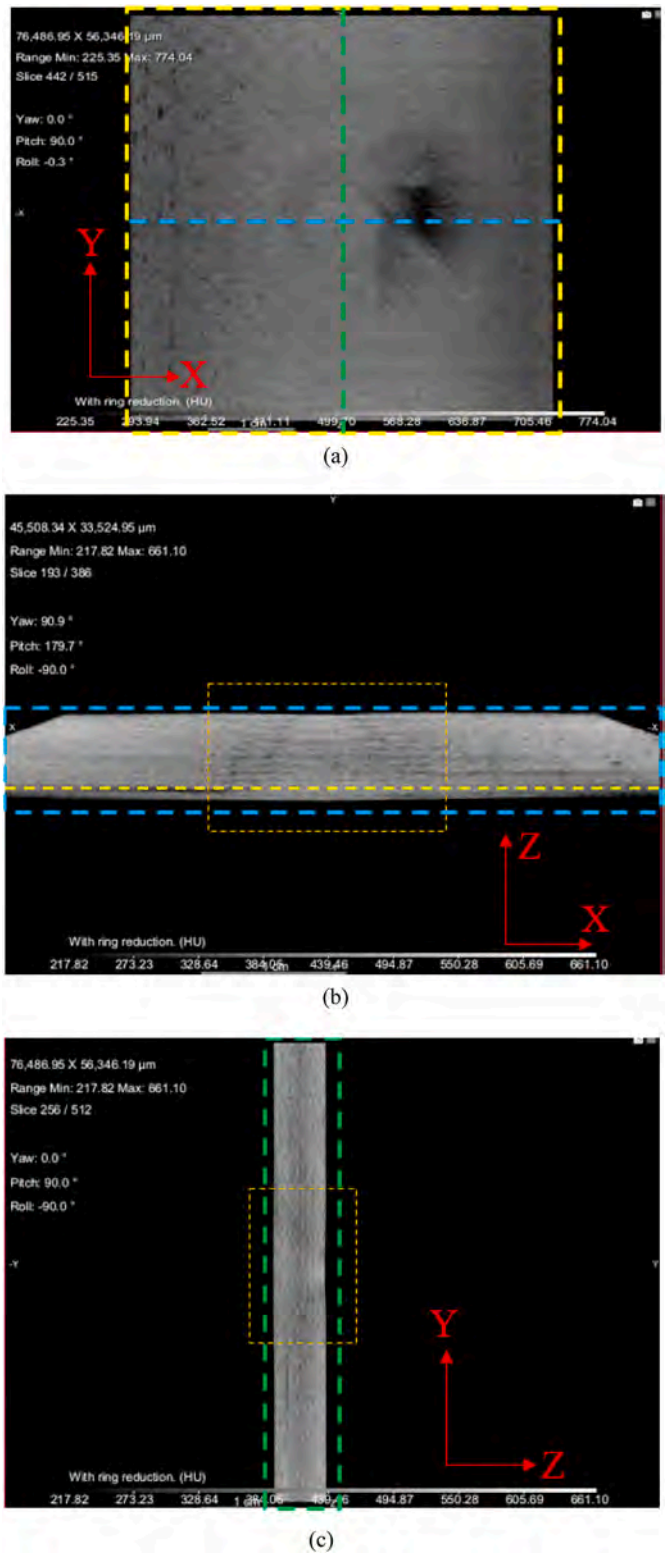

Fig. 35. X-ray micro-CT of 6 mm coupon with 1″ impact damage.

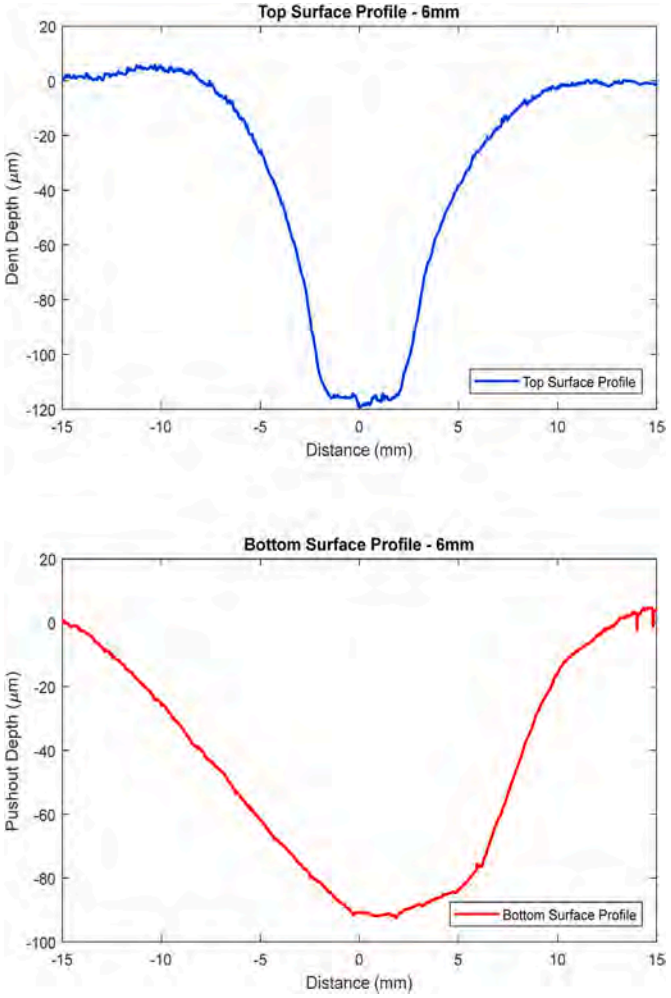

Fig. 36. Profilometry scans of 6-mm coupon: (a) top surface; (b) bottom surface.

6.3. *FUTURE WORK*

We would like to translate the findings in this paper to advanced thermoplastic composites of different thicknesses to achieve close to 1″ impact damage diameter. We would also explore the possibility of deviating from the ASTM standard of impact testing by utilizing impactor tups of smaller (0.5″) or larger (1”) sizes. Instrumented coupons with piezoelectric wafer active sensors (PWAS) will also be utilized to perform in-situ acoustic emission (AE) tests that will be used to ascertain if damage has occurred in impacted composites or not. Methods of obtaining controlled impact damage sizes will also be utilized in exploring guided-wave structural health monitoring (SHM) techniques of real impact damage instead of improperly simulated impact damage using multiple embedded delaminations employing

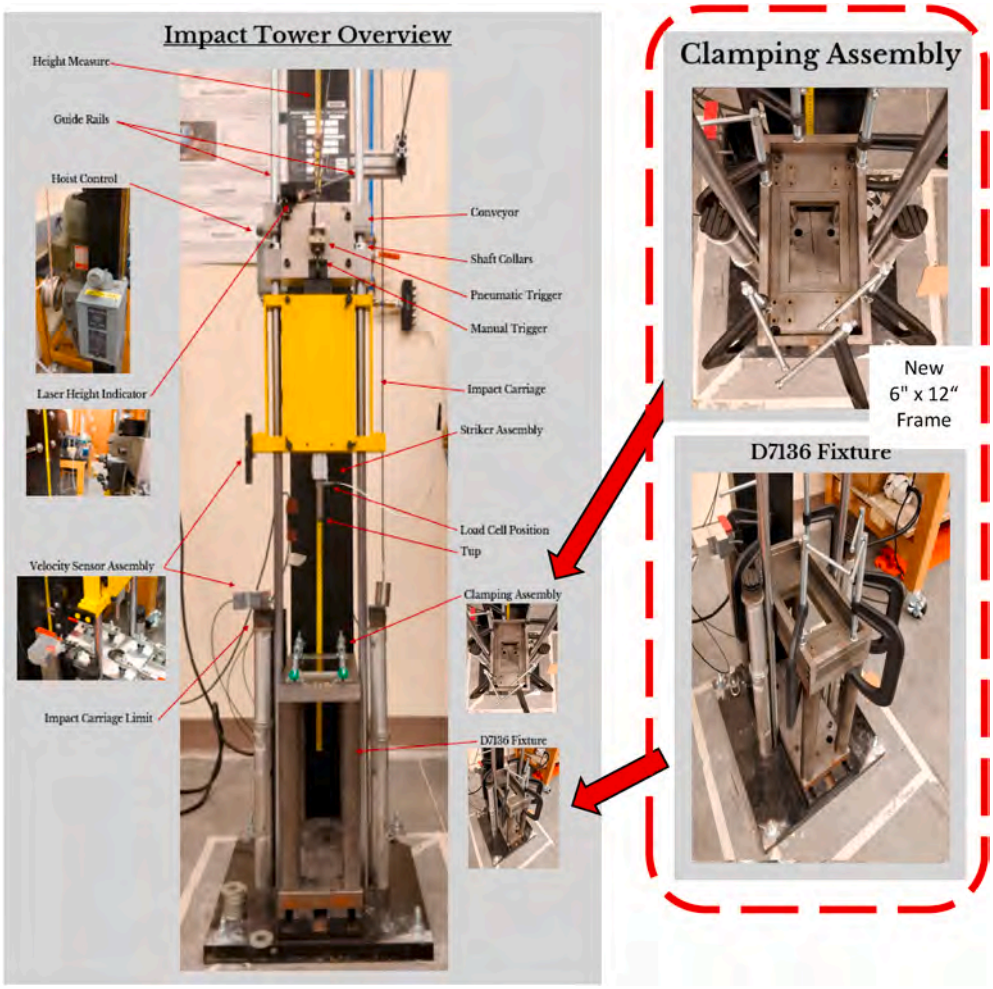

Fig. 37. Proposed modification of the coupon holding fixture on the Dynatup 8200 drop weight impact testing machine.

Table 4
Impact tests conducted on 12″ × 6″, 6-mm quasi-isotropic coupons.

Coupon	Avg. thickness (mm)	Mass (kg)	Height (cm)	Energy (J)	Impact velocity (m/s)	Momentum (Ns)	Damage size (in)	Ei (J)	% of Ei absorbed
QL6A	6.23	5.406	41.110	21.802	2.911	15.74	0.095	22.91	52%
QL6A	6.23	5.406	61.666	32.703	3.600	19.46	2.2	35.03	74%
QL6B	6.25	5.406	51.388	27.253	3.322	17.96	0.4	29.82	49%
QL6B	6.25	5.406	56.527	29.978	3.429	18.54	2	31.78	73%
QL6C	6.26	5.406	53.957	28.615	3.402	18.39	0.45	31.28	51%
QL6C	6.26	5.406	55.242	29.297	3.365	18.19	2	30.60	68%
QL6D	6.23	5.406	56.527	29.978	3.430	18.54	0.37	31.79	49%

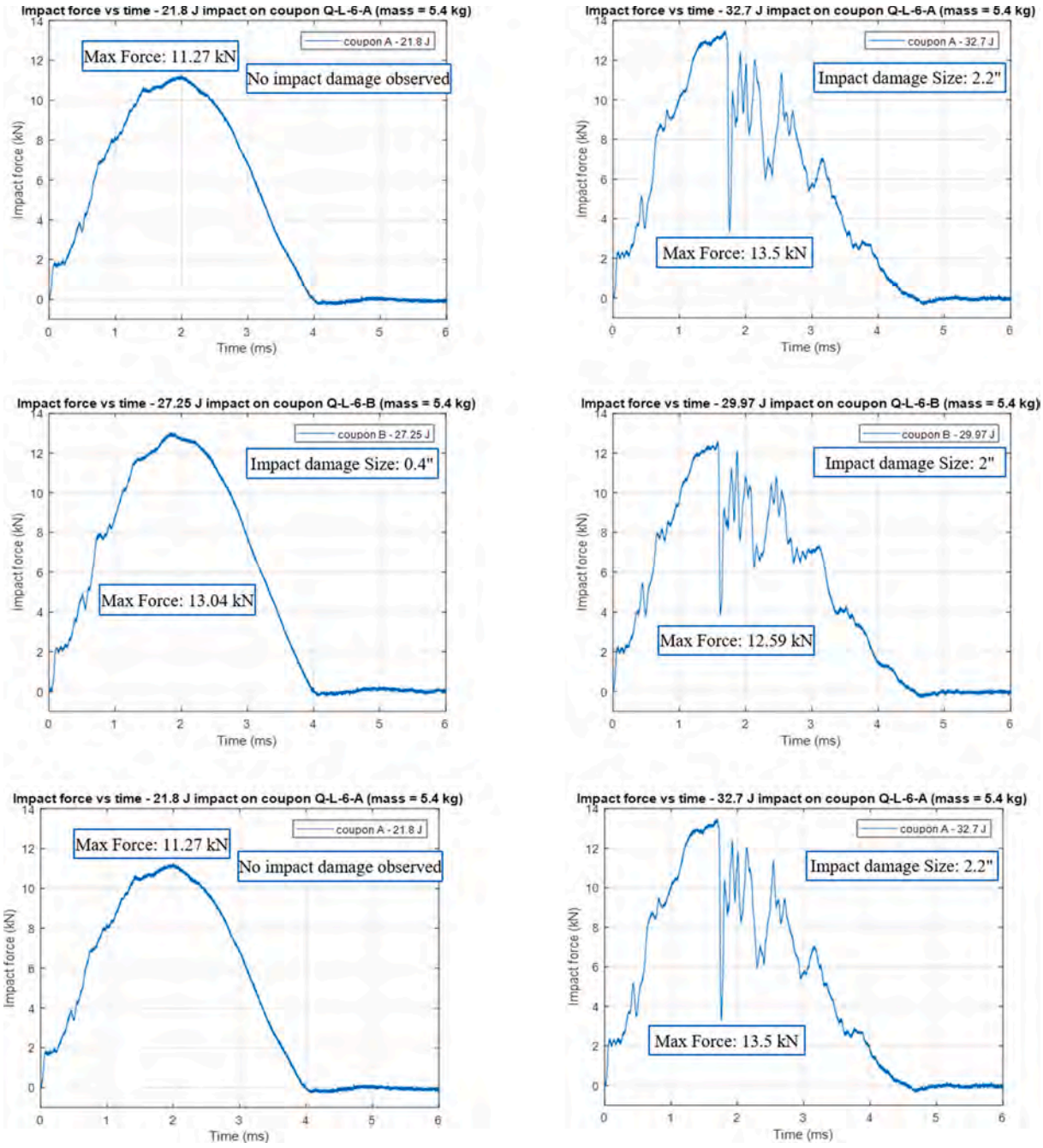

Fig. 38. Force-time histories of coupons QL6A, QL6B and QL6C for double impacts.

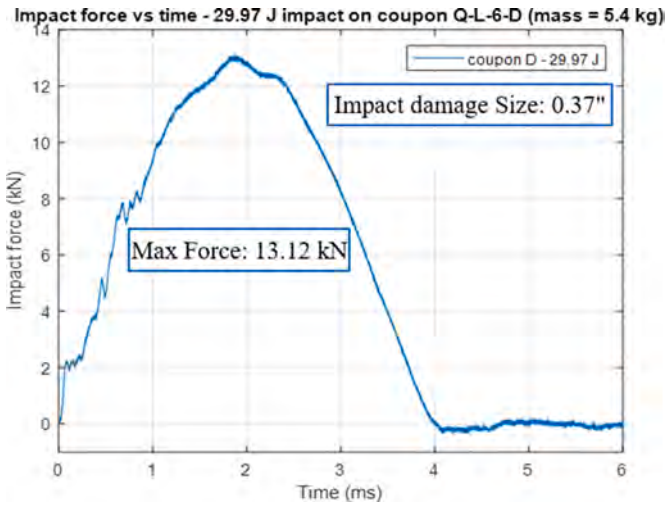

Fig. 39. Force-time history of coupons QL6D for single impact.

materials such as Teflon or Mylar which do not simulate the real impact damage. Impact damage patterns from current experiments will be utilized in modeling the impact damage for guided wave propagation simulations for comparisons with laboratory experiments.

CRediT authorship contribution statement

Robin James: Software, Data curation, Investigation, Validation, Visualization, Writing - original draft, Writing - review & editing. **Victor Giurgiutiu:** Conceptualization, Methodology, Supervision, Writing - review & editing.

Declaration of competing interest

The authors declare that they have no known competing financial interests or personal relationships that could have appeared to influence the work reported in this paper.

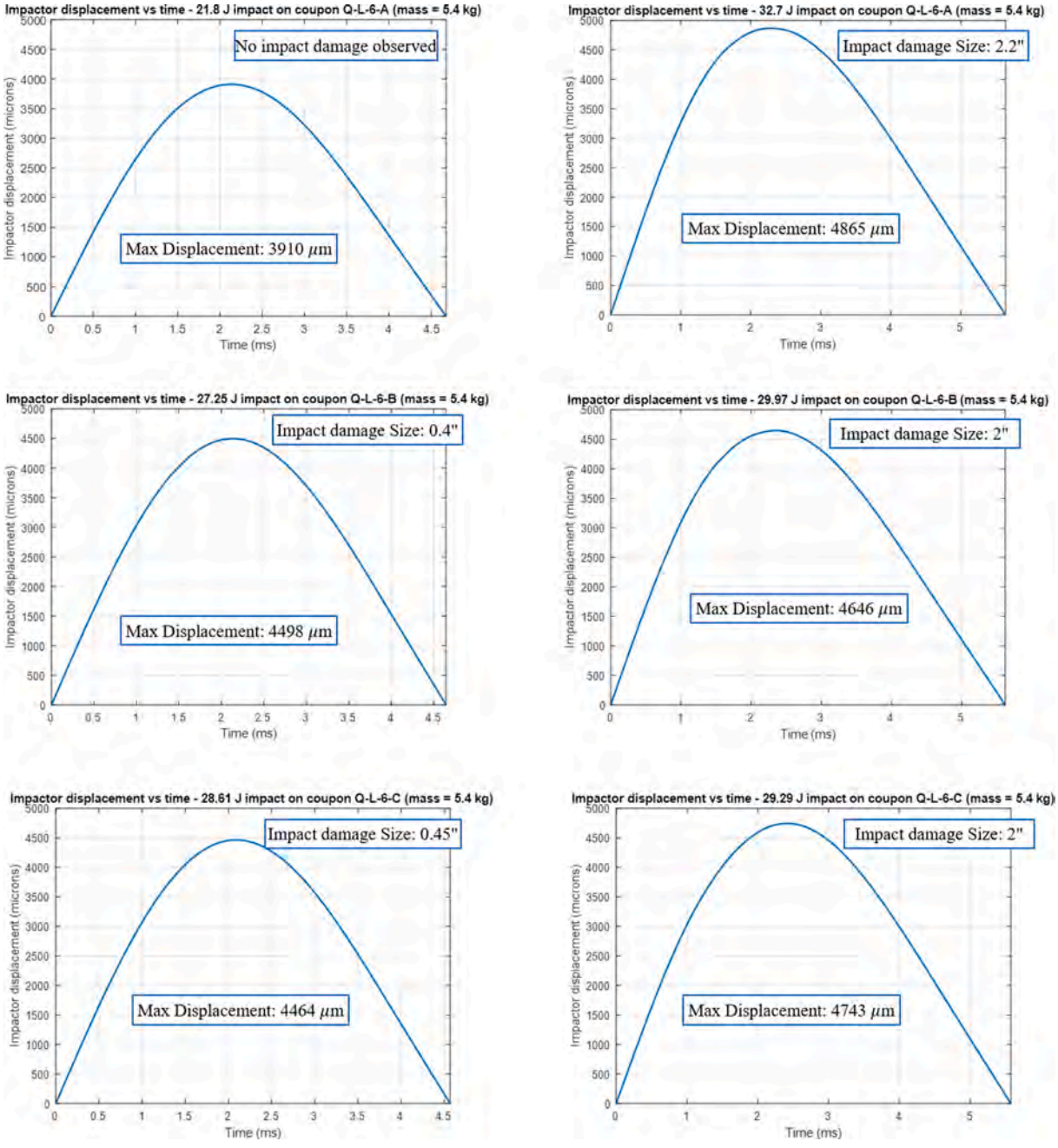

Fig. 40. Displacement-time histories of coupons QL6A, QL6B and QL6C.

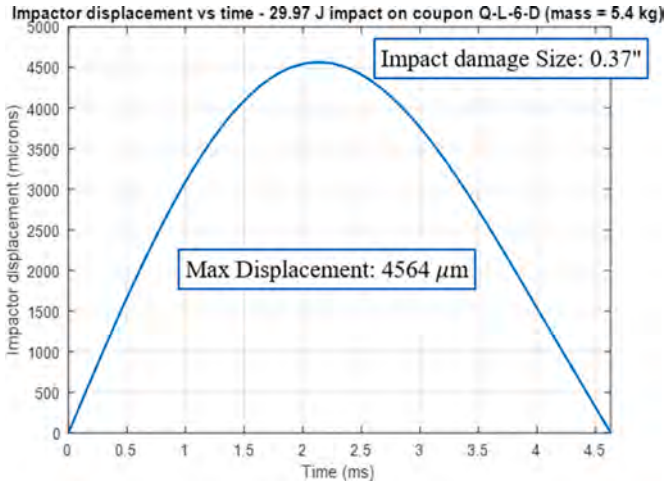

Fig. 41. Displacement-time history of coupons QL6D.

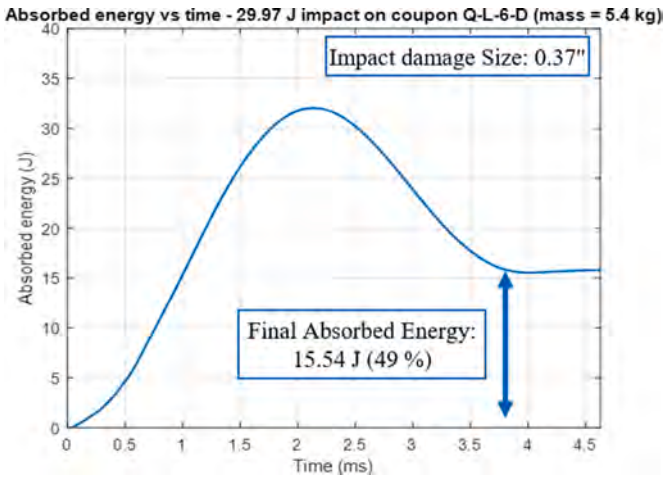

Fig. 43. Energy-time history of coupons QL6D.

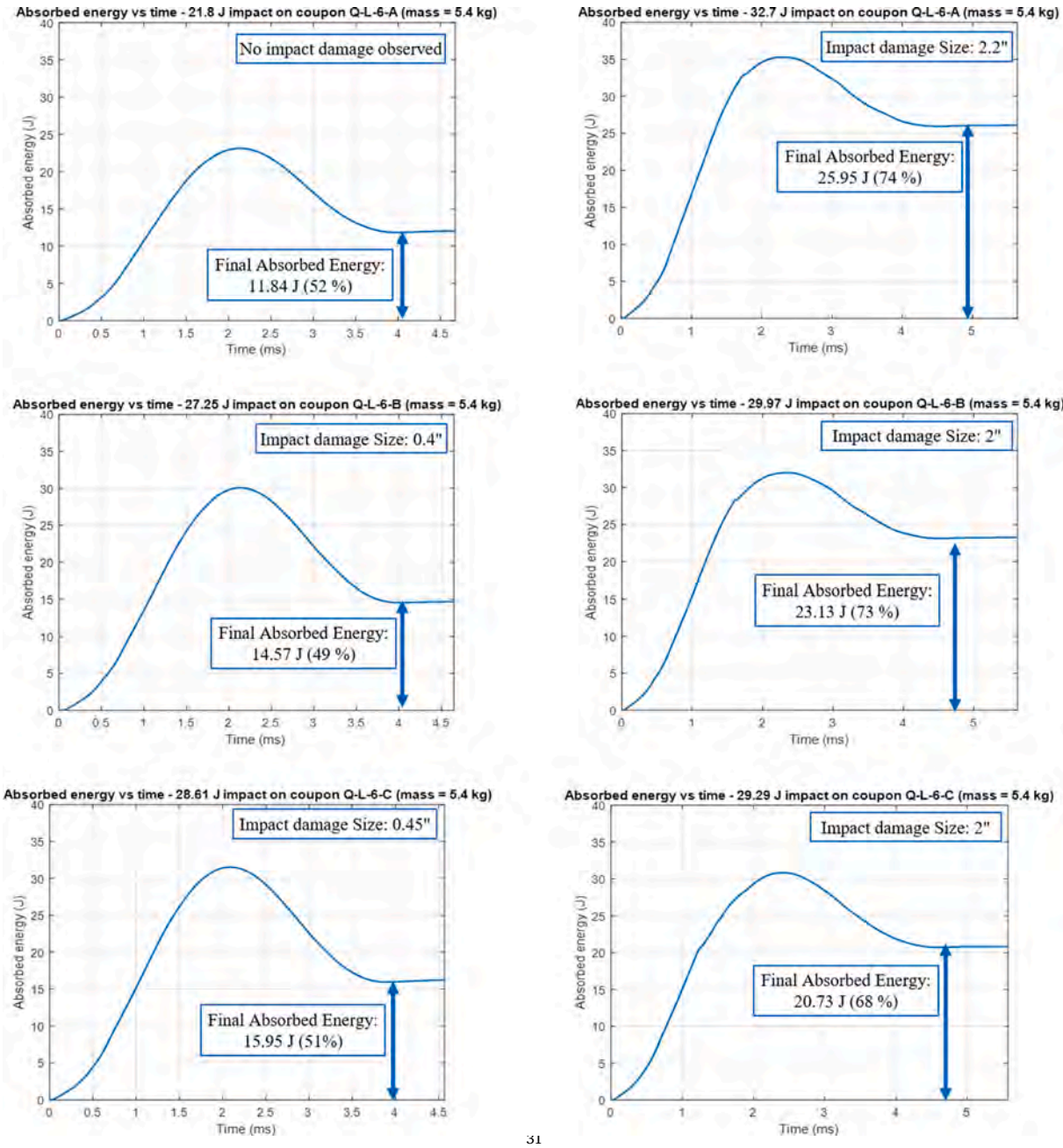

Fig. 42. Energy-time histories of coupons QL6A, QL6B and QL6C.

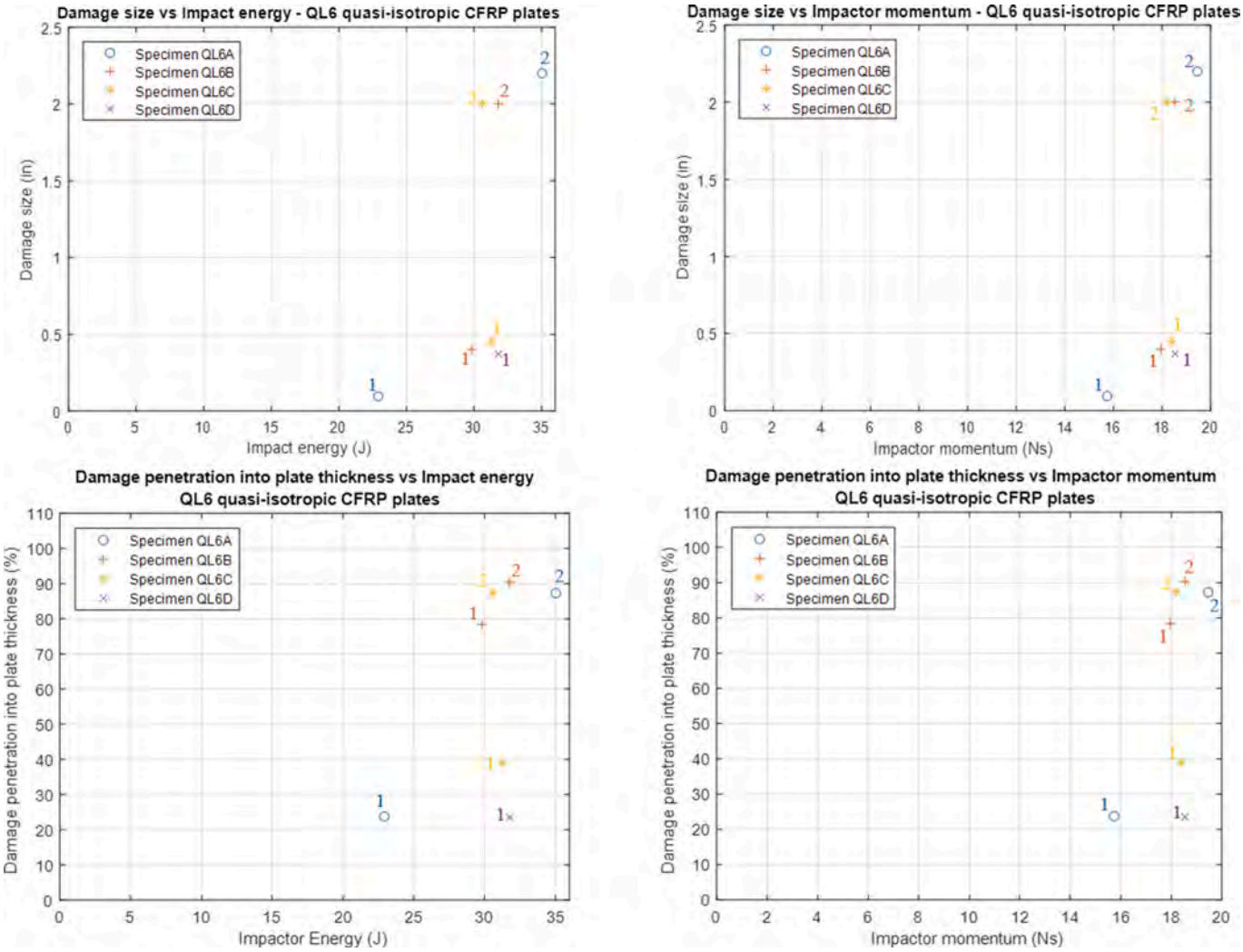

Fig. 44. Effect of impact energy and momentum on impact damage size and damage penetration across the thickness for coupons QL6A, QL6B, QL6C and QL6D.

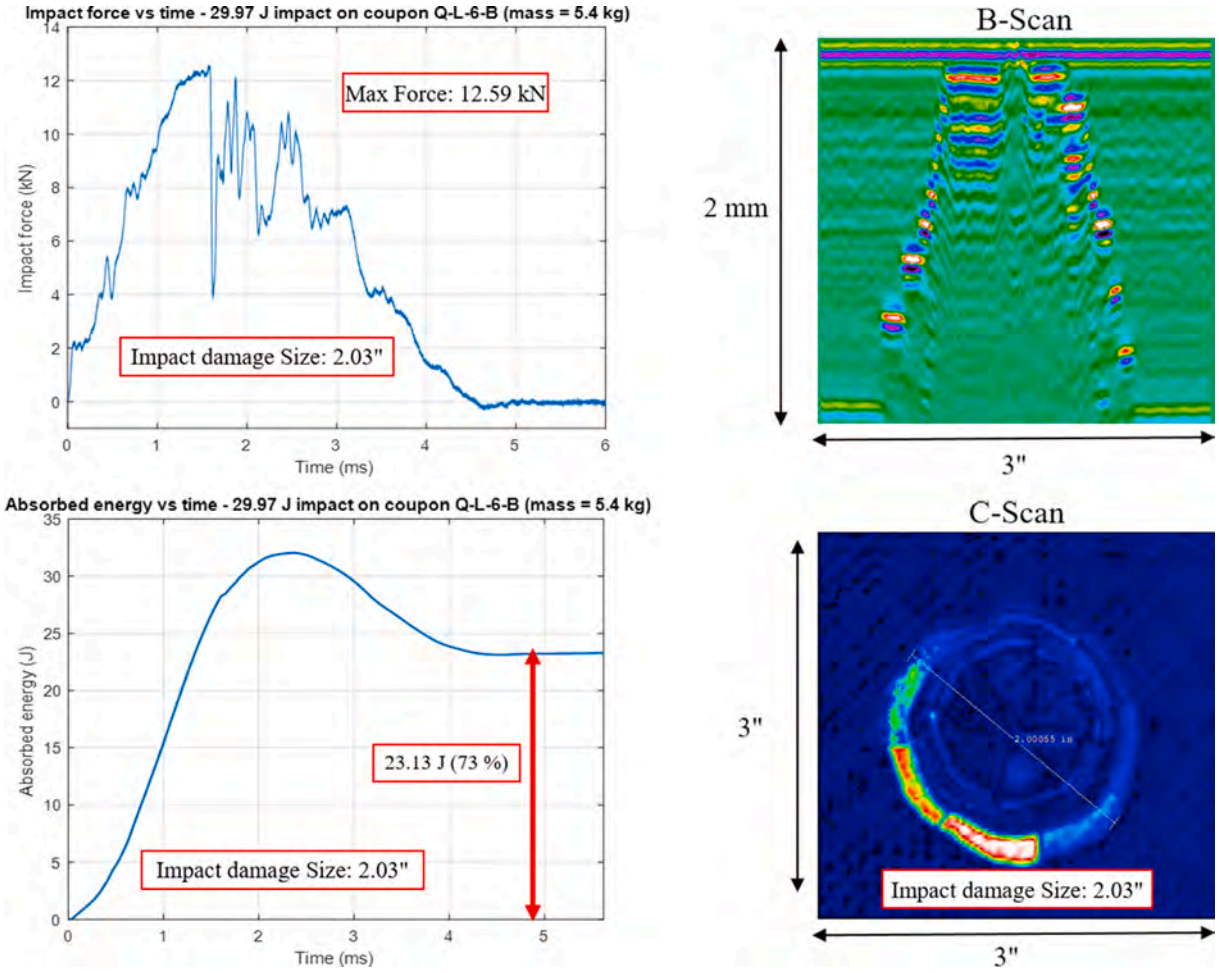

Fig. 45. Quad plot of QL6B coupon with force-history, energy-history, B-scan and C-scan.

Acknowledgements

This work was supported by the Air Force Office of Scientific Research (AFOSR) grant number FA9550-16-1-0401. The authors would like to thank the Ronald E. McNair Center for Aerospace Innovation and Research for providing them the manufacturing facilities to manufacture the composite coupons. The authors would also like to thank Dr. Xinyu Huang for providing the drop-weight impact tower for conducting the ASTM D7136 impact tests. The support of the University of South Carolina's School of Medicine instrumentation Resource facility for providing the X-ray microCT facility is greatly appreciated.

The authors greatly appreciate Dr. Vipul Ranatunga and Dr. Stephen Clay from the Air Force Research Laboratory (AFRL) for their useful and constructive advice they have provided during experiments and interpretation of the experimental data.

References

[1] Butcher BR. The impact resistance of unidirectional CFRP under tensile stress. Fibre Sci Technol 1979;12(4):295–326.
[2] Toland R. Impact testing of carbon-epoxy composite materials. In: DeSisto T, editor. Instrumented impact testing. West Conshohocken, PA: ASTM International; 1974. p. 133–45.
[3] Cantwell WJ, Morton J. Comparison of the low and high velocity impact response of CFRP. Composites 1989;20(6):545–51.
[4] Cantwell WJ, Curtis PT, Morton J. An assessment of the impact performance of CFRP reinforced with high-strain carbon fibres. Compos Sci Technol 1986;25(2):133–48.
[5] Cantwell WJ, Morton J. Geometrical effects in the low velocity impact response of CFRP. Compos Struct 1989;12(1):39–59.
[6] Cantwell WJ. The influence of target geometry on the high velocity impact response of CFRP. Compos Struct 1988;10(3):247–65.
[7] Cantwell WJ, Morton J. The influence of varying projectile mass on the impact response of CFRP. Compos Struct 1989;13(2):101–14.
[8] Cantwell WJ, Morton J. Detection of impact damage in CFRP laminates. Compos Struct 1985;3(3–4):241–57.
[9] ASTM D7136. Standard test method for measuring the damage resistance of a fiber-reinforced-polymer matrix composites to a drop-weight impact event, vol. 15. Book of Standards; 2005.
[10] Ishai O, Shragai A. Effect of impact loading on damage and residual compressive strength of CFRP laminated beams. Compos Struct 1990;14(4):319–37.
[11] Stellbrink K. On the behaviour of impact damaged CFRP laminates. Fibre Sci Technol 1983;18(2):81–94.
[12] Caprino G. Residual strength prediction of impacted CFRP laminates. J Compos Mater 1984;18(6):508–18.
[13] Clark G. Modelling of impact damage in composite laminates. Composites 1989;20(3):209–14.
[14] Sun C. An analytical method for evaluation of impact damage energy of laminated composites. In: Davis J, editor. Composite materials: testing and design (fourth conference). West Conshohocken, PA: ASTM International; 1977. p. 427–40.
[15] Greszczuk L, Chao H. Impact damage in graphite-fiber-reinforced composites. In: Davis J, editor. Composite materials: testing and design (fourth conference). West Conshohocken, PA: ASTM International; 1977. p. 389–408.
[16] Bonini J, Collombet F, Lataillade JL. Numerical modelling of contact for low velocity impact damage in composite laminates. WIT Trans Eng Sci 1970;1.
[17] Becker W. Mathematical simulation of external and internal damage due to low velocity impact. WIT Trans Eng Sci 1970;4.
[18] Schoeppner GA, Abrate S. Delamination threshold loads for low velocity impact on composite laminates. Compos Appl Sci Manuf 2000;31(9):903–15.
[19] Caputo F, De Luca A, Lamanna G, Borrelli R, Mercurio U. Numerical study for the structural analysis of composite laminates subjected to low velocity impact. Compos B Eng 2014;67:296–302.
[20] Flores M, Mollenhauer D, Runatunga V, Beberniss T, Rapking D, Pankow M. High-speed 3D digital image correlation of low-velocity impacts on composite plates. Compos B Eng 2017;131:153–64.

[21] Wallentine SM, Uchic MD. A study on ground truth data for impact damaged polymer matrix composites. AIP conference proceedings, vol. 1949. AIP Publishing; 2018. p. 120002. , No. 1.
[22] Bogenfeld R, Kreikemeier J, Wille T. Review and benchmark study on the analysis of low-velocity impact on composite laminates. Eng Fail Anal 2018;86:72–99.
[23] Panettieri E, Fanteria D, Montemurro M, Froustey C. Low-velocity impact tests on carbon/epoxy composite laminates: a benchmark study. Compos B Eng 2016;107:9–21.
[24] Gómez-del Río T, Zaera R, Barbero E, Navarro C. Damage in CFRPs due to low velocity impact at low temperature. Compos B Eng 2005;36(1):41–50.
[25] Sutherland LS, Guedes Soares C. Impact behaviour of typical marine composite laminates. Compos B Eng 2005;37(2–3):89–100.
[26] Sevkat E, Liaw B, Delale F, Raju BB. Effect of repeated impacts on the response of plain-woven hybrid composites. Compos B Eng 2010;41(5):403–13.
[27] Amaro AM, Reis PNB, De Moura MFSF, Neto MA. Influence of multi-impacts on GFRP composites laminates. Compos B Eng 2013;52:93–9.
[28] Olsson R. Analytical prediction of large mass impact damage in composite laminates. Compos Appl Sci Manuf 2001;32(9):1207–15.
[29] Ghajari M, Sharif-Khodaei Z, Aliabadi MH, Apicella A. Identification of impact force for smart composite stiffened panels. Smart Mater Struct 2013;22(8):085014.
[30] Davis MJ, Jones R. Damage tolerance of fibre composite laminates. Fracture mechanics technology applied to material evaluation and structure design. Dordrecht: Springer; 1983. p. 635–55.
[31] Anderson BW. Factors affecting the design of military aircraft structures in carbon fibre reinforced composites. Fracture 1984;84:607–22. Pergamon.
[32] MIL-HDBK-17-3F. Composite materials handbook 2002;3:7–29 [chapter 7].
[33] Bar-Cohen Y, Crane RL. U.S. Patent No. 4,457,174. Washington, DC: U.S. Patent and Trademark Office; 1984.
[34] Aymerich F, Meili S. Ultrasonic evaluation of matrix damage in impacted composite laminates. Compos B Eng 2000;31(1):1–6.
[35] Gresil M, Giurgiutiu V. Guided wave propagation in composite laminates using piezoelectric wafer active sensors. Aeronaut J 2013;117(1196):971–95.
[36] Santos MJ, Santos JB, Amaro AM, Neto MA. Low velocity impact damage evaluation in fiber glass composite plates using PZT sensors. Compos B Eng 2013;55:269–76.
[37] Tai S, Kotobuki F, Wang L, Mal A. Modeling ultrasonic elastic waves in fiber-metal laminate structures in presence of sources and defects. Journal of Nondestructive Evaluation, Diagnostics and Prognostics of Engineering Systems 2020;3(4).
[38] Rogge MD, Leckey CA. Characterization of impact damage in composite laminates using guided wavefield imaging and local wavenumber domain analysis. Ultrasonics 2013;53(7):1217–26.
[39] James R, Faisal Haider M, Giurgiutiu V, Lilienthal D. A simulative and experimental approach toward eddy current nondestructive evaluation of manufacturing flaws and operational damage in CFRP composites. Journal of Nondestructive Evaluation, Diagnostics and Prognostics of Engineering Systems 2020;3(1).
[40] Liang T, Ren W, Tian GY, Elradi M, Gao Y. Low energy impact damage detection in CFRP using eddy current pulsed thermography. Compos Struct 2016;143:352–61.
[41] He Y, Tian G, Pan M, Chen D. Impact evaluation in carbon fiber reinforced plastic (CFRP) laminates using eddy current pulsed thermography. Compos Struct 2014;109(1):1–7.
[42] Narayanan RM, James R. Microwave nondestructive testing of galvanic corrosion and impact damage in carbon fiber reinforced polymer composites. Int J Microw Appl 2018;7(1):1–15.
[43] Li Z, Haigh AD, Soutis C, Gibson AAP. Simulation for the impact damage detection in composites by using the near-field microwave waveguide imaging. In: NDT 2014 - 53rd annual conference of the British institute of non-destructive testing. British Institute of Non-Destructive Testing; 2014.
[44] Greenawald EC, Levenberry LJ, Qaddoumi N, McHardy A, Zoughi R, Poranski Jr CF. Microwave NDE of impact damaged fiberglass and elastomer layered composites. AIP conference proceedings, vol. 509. American Institute of Physics; 2000. p. 1263–8. No. 1.
[45] Li Z, Soutis C, Haigh A, Sloan R, Gibson A. Application of an electromagnetic sensor for detection of impact damage in aircraft composites. In: *2016* 21st international conference on microwave, radar and wireless communications, MIKON 2016. Institute of Electrical and Electronics Engineers Inc; 2016.
[46] Meola C, Carlomagno GM. Impact damage in GFRP: new insights with infrared thermography. Compos Appl Sci Manuf 2010;41(12):1839–47.
[47] Tan KT, Watanabe N, Iwahori Y. X-ray radiography and micro-computed tomography examination of damage characteristics in stitched composites subjected to impact loading. Compos B Eng 2011;42(4):874–84.
[48] Meola C, Carlomagno GM. Infrared thermography to evaluate impact damage in glass/epoxy with manufacturing defects. Int J Impact Eng 2014;67:1–11.
[49] Bull DJ, Helfen L, Sinclair I, Spearing SM, Baumbach T. A comparison of multi-scale 3D X-ray tomographic inspection techniques for assessing carbon fibre composite impact damage. Compos Sci Technol 2013;75:55–61.
[50] Schilling PJ, Karedla BR, Tatiparthi AK, Verges MA, Herrington PD. X-ray computed microtomography of internal damage in fiber reinforced polymer matrix composites. Compos Sci Technol 2005;65(14):2071–8.
[51] Mei H, Haider MF, James R, Giurgiutiu V. Pure S0 and SH0 detections of various damage types in aerospace composites. Compos B Eng 2020;189:107906.
[52] Mei H, James R, Haider MF, Giurgiutiu V. Multimode guided wave detection for various composite damage types. Appl Sci 2020;10(2):484.
[53] James R, Mei H, Giurgiutiu V. April). SH-mode guided-wave impact damage detection in thick quasi-isotropic composites. Health monitoring of structural and biological systems IX, vol. 11381. International Society for Optics and Photonics; 2020. p. 113810R.
[54] Mei H, James R, Giurgiutiu V. Damage detection in laminated composites using pure SH guided wave excited by angle beam transducer. Health monitoring of structural and biological systems IX, vol. 11381. International Society for Optics and Photonics; 2020. p. 113810P.
[55] James R, Joseph R, Giurgiutiu V. Impact damage detection in composite plates using acoustic emission signal signature identification (Conference Presentation). Active and passive smart structures and integrated systems IX, vol. 11376. International Society for Optics and Photonics; 2020. p. 113760K.
[56] James R, Giurgiutiu V, Flores M. Challenges of generating controlled one-inch impact damage in thick CFRP composites. American Institute of Aeronautics and Astronautics (AIAA); 2020.
[57] Moradi M, Safizadeh MS. Experimental and numerical study of the effect of using polyurethane instead of Teflon strip to simulate debonding defect in composite patch repairs aluminum plate under thermography inspection. Compos B Eng 2019;175.